J Oceanogr (2015) 71:469–497
DOI 10.1007/s10872-015-0283-7

SPECIAL SECTION: REVIEW

"Hot Spots" in the Climate System: New Developments in the Extratropical Ocean-Atmosphere Interaction Research

Oceanic fronts and jets around Japan: a review

Shinichiro Kida[1] · Humio Mitsudera[2] · Shigeru Aoki[2] · Xinyu Guo[3] · Shin-ichi Ito[4] · Fumiaki Kobashi[5] · Nobumasa Komori[1] · Atsushi Kubokawa[6] · Toru Miyama[1] · Ryosuke Morie[7] · Hisashi Nakamura[1,8] · Tomohiro Nakamura[2] · Hideyuki Nakano[9] · Hajime Nishigaki[10] · Masami Nonaka[1] · Hideharu Sasaki[1] · Yoshi N. Sasaki[11] · Toshio Suga[12] · Shusaku Sugimoto[12] · Bunmei Taguchi[1] · Koutarou Takaya[13] · Tomoki Tozuka[14] · Hiroyuki Tsujino[9] · Norihisa Usui[9]

Received: 17 July 2014 / Revised: 26 February 2015 / Accepted: 9 March 2015 / Published online: 8 April 2015

Abstract This article reviews progress in our understanding of oceanic fronts around Japan and their roles in air–sea interaction. Fronts associated with the Kuroshio and its extension, fronts within the area of the Kuroshio-Oyashio confluence, and the subtropical fronts are described with particular emphasis on their structure, variability, and role in air–sea interaction. The discussion also extends to the fronts in the coastal and marginal seas, the Seto Inland Sea and Japan Sea. Studies on oceanic fronts have progressed significantly during the past decade, but many of these studies focus on processes at individual fronts and do not provide a comprehensive view. Hence, one of the goals of this article is to review the oceanic fronts around Japan by describing the processes based on common metrics. These metrics focus primarily on surface properties to obtain insights into air–sea interactions that occur along oceanic fronts. The basic characteristics derived for each front (i.e., metrics) are then presented as a table. We envision that many of the coupled ocean-atmosphere global circulation models in the coming decade will represent oceanic fronts reasonably well, and it is hoped that this review along with the table of metrics will provide a useful benchmark for evaluating these models.

Keywords Oceanic fronts · Western North Pacific · Air–sea interaction · Kuroshio Extension · Kuroshio-Oyashio confluence region · Subtropical fronts

1 Oceanic fronts and their roles in climate

Scientific studies of oceanic fronts have a long and rich history in the field of oceanography since the first half of the twentieth century. In Japan, oceanic fronts were referred to as "shiome" (e.g., Uda 1938) and have been studied extensively because of their importance for fisheries. Kitahara

✉ Shinichiro Kida
kidas@jamstec.go.jp

1 Application Laboratory, Japan Agency for Marine-Earth Science and Technology, 3173-25 Showa-machi, Kanazawa-ku, Yokohama 236-0001, Japan

2 Institute of Low Temperature Science, Hokkaido University, Sapporo, Japan

3 Center for Marine Environmental Studies, Ehime University, Matsuyama, Japan

4 Atmosphere and Ocean Research Institute, The University of Tokyo, Kashiwa, Japan

5 Graduate School of Marine Science and Technology, Tokyo University of Marine Science and Technology, Tokyo, Japan

6 Faculty of Environmental Earth Science, Hokkaido University, Sapporo, Japan

7 Graduate School of Environmental Science, Hokkaido University, Sapporo, Japan

8 Research Center for Advanced Science and Technology, The University of Tokyo, Tokyo, Japan

9 Meteorological Research Institute, Tsukuba, Japan

10 Faculty of Education and Welfare Science, Oita University, Oita, Japan

11 Graduate School of Science, Hokkaido University, Sapporo, Japan

12 Department of Geophysics, Graduate School of Science, Tohoku University, Sendai, Japan

13 Faculty of Science, Kyoto Sangyo University, Kyoto, Japan

14 Department of Earth and Planetary Science, Graduate School of Science, The University of Tokyo, Tokyo, Japan

(1921) proposed what is known today as Kitahara's law: fish tend to aggregate around fronts. The importance of fronts led to the initiation of operational oceanography in Japan in 1935, with oceanic conditions and fishing ground positions analyzed routinely from oceanic temperature and fish-catch data collected from fishing boats, which were broadcasted through the NHK (Japan Broadcasting Corp.) radio (Kimura 1949). Oceanic fronts were called "tidal rips" or "current rips" in English. In recognition of its similarity to an atmospheric front, Cromwell and Reid (1956) first introduced the term "oceanic front" defined as "a band along the sea surface across which the density changes abruptly." Today, the term "oceanic front" is used in a somewhat broader sense as an oceanic zone with a strong horizontal gradient in water properties such as temperature, salinity, etc.

Oceanic fronts are ubiquitous with various magnitudes and spatial scales. On the large scale, fronts form along oceanic jets, such as the Kuroshio Extension (KE), and through coastal upwelling. On a smaller scale, fronts form through tides, freshwater input from rivers, and along continental shelf breaks. While many studies have investigated their formation mechanisms, some oceanic fronts along jets have recently gained interest as locations of subduction where the oceanic interior exchanges properties with the surface mixed layer (Pollard and Regier 1992). Since subduction plays a critical role in determining the dynamical properties and stratification of the ocean interior (e.g., Joyce and Jenkins 1993; Spall 1995), full understanding of this mechanism has thus been considered one of the fundamental problems for understanding the global oceanic circulation (see Talley et al. 2011 and reference therein).

Today, extra-tropical oceanic fronts are recognized in the climate system as narrow zones of vigorous air–sea coupling that occurs through the modification of the planetary boundary layer (PBL) (Xie 2004; Small et al. 2008; Kelly et al. 2010). Across an oceanic front, differential heat release into the atmosphere yields cross-frontal contrasts in stratification and thus vertical mixing by turbulence within the PBL, influencing the downward transport of wind momentum to the surface (Wallace et al. 1989; Hayes et al. 1989). The frontal influence on the surface wind-speed through the modulated vertical mixing depends on the wind direction relative to the frontal axis (Chelton et al. 2004). A front can modify cross-frontal winds acting to yield surface convergence/divergence, whereas surface wind curl can be generated for winds along the frontal axis. The modulation of surface winds could be complicated under the strong low-level thermal winds (Tanimoto et al. 2011). Differential heat release across an oceanic front also modifies thermal conditions in the PBL and thereby surface pressure via the hydrostatic effect (Lindzen and Nigam 1987), with frictional surface convergence over locally warm water (Tanimoto et al. 2011). This hydrostatic effect has been shown to be operative ubiquitously along the major warm western boundary currents (Shimada and Minobe 2011). With such frictional near-surface wind convergence at work, locally enhanced heat and moisture supplied by a warm western boundary current can lead to organization of convective cloud systems along the current, as shown in recent observational and numerical studies (Minobe et al. 2008, 2010; Kuwano-Yoshida et al. 2010; Miyama et al. 2012).

While identifying solid evidence of air–sea coupling on the large-scale atmospheric circulation has been challenging, significant advances have been made during the past decade by uncovering the potential impacts of the sea surface temperature (SST) fronts on the free troposphere (e.g., Nakamura et al. 2004; Minobe et al. 2008; Kwon et al. 2010). The vigorous heat and moisture release into the atmosphere near oceanic fronts and their sharp cross-frontal contrast (Fig. 1) are beginning to be accepted as an essential feature of the extra-tropical climate (Hoskins 2012; Imawaki et al. 2013). In fact, decadal-scale variability of the SST in the extratropical North Pacific is known to be concentrated on oceanic frontal zones (e.g., Nakamura et al. 1997; Nakamura and Kazmin 2003). By modulating heat supply into the atmosphere (Tanimoto et al. 2003), persistent SST anomalies generated along the oceanic frontal zone in the western North Pacific with its meridional displacement have the potential to force a large-scale atmospheric anomaly recognized as the anomalous Aleutian Low (Frankignoul et al. 2011; Taguchi et al. 2012; Okajima et al. 2014) through modulating storm-track activity.

In this article, we aim to provide a review of dynamical studies on some of the oceanic fronts that exist in the western North Pacific (Figs. 1, 2). We will focus mainly on those associated with the western boundary currents, such as the Kuroshio and Oyashio, and jets that lie in the interior, such as the KE, those in the area of the Kuroshio-Oyashio confluence [referred to as the Kuroshio-Oyashio confluence (KOC) region hereafter; see Sect. 4 for details on the terminology of this region], and subtropical fronts (STFs). Some of the coastal and marginal-sea scale features around Japan will also be discussed. While we cannot completely cover all of the fronts around Japan, many fronts in the western North Pacific have received extensive attention because of the "Hot Spot in Climate System" Project (Nakamura 2012), and significant progress has been made on various aspects. Since the knowledge of fronts around Japan has not been collectively discussed since Uda (1938), we hope that this article will be a step toward synthesizing what has accumulated separately at each front and updating some of the recent findings on their impact on the atmosphere. As one of the tools for examining the fronts comprehensively and qualitatively,

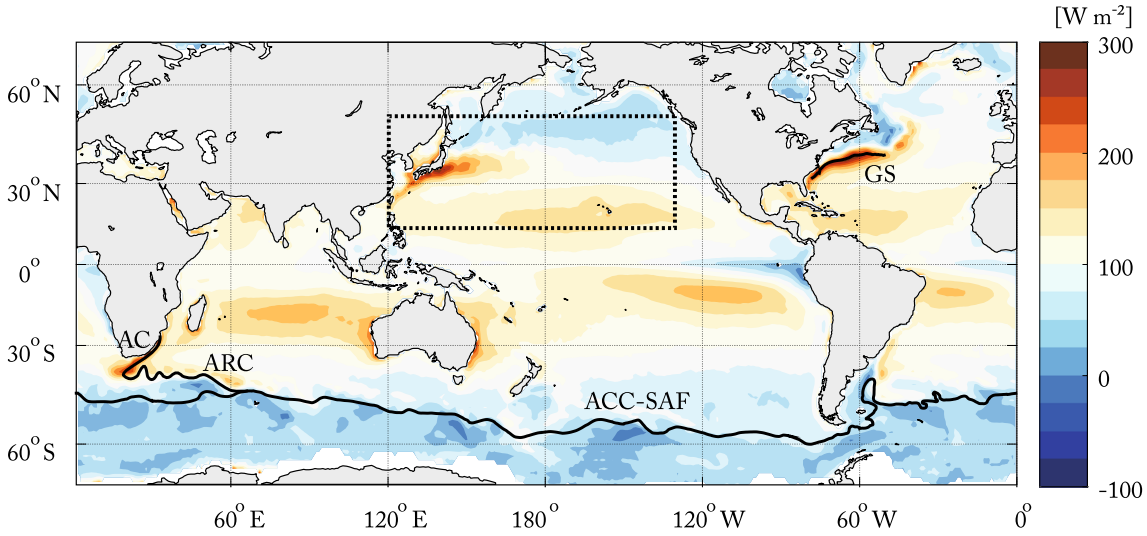

Fig. 1 Global distribution of the sum of latent and sensible heat fluxes based on the J-OFURO2 (1993–2007). The region of the fronts focused on in this article is the *squared dotted lines* and is shown in Fig. 2. The locations of the Gulf Stream, Agulhas Current, Agulhas Return Current, and Subantarctic Front are shown by *black solid lines*, where they show some resemblance to the western North Pacific as a region of enhanced heat fluxes

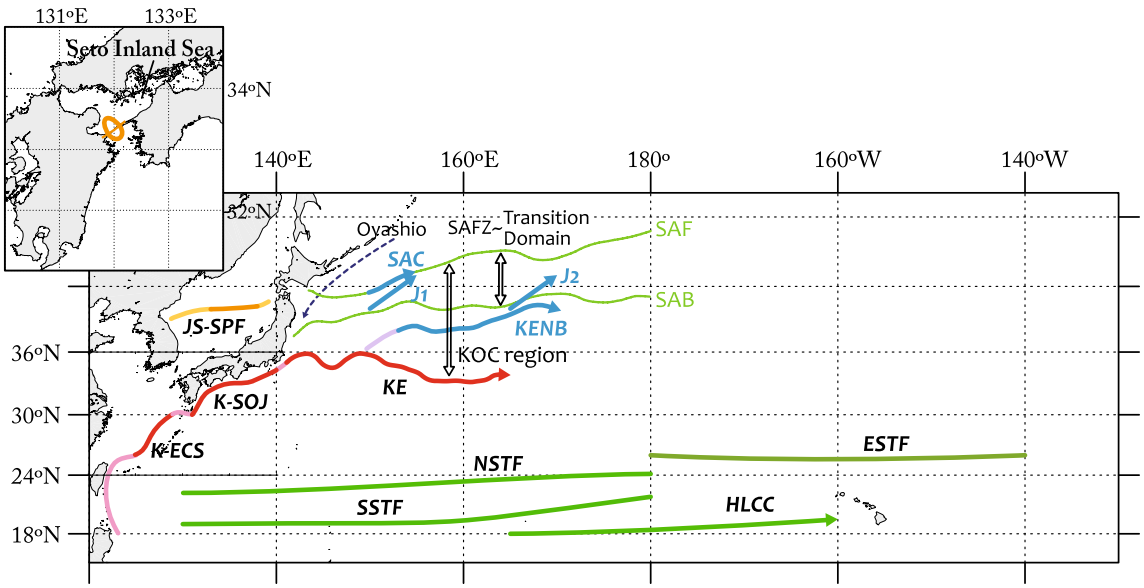

Fig. 2 Geographical locations of oceanic fronts over the western North Pacific that are described in this article. The *inset* shows the tidal front in the Seto Inland Sea of Japan. The start and end of the *frontal lines* are those in Tables 1, 2, 3, 4, and 5, and the *arrows* correspond to the direction of the currents along the frontal axis. As indicated with *different colors*, the fronts are grouped together based on the sections in this article. *Light-colored lines* are drawn to illustrate the connection of fronts. The names of the fronts are abbreviated as indicated in Tables 1, 2, 3, 4, and 5. SAB is the subarctic boundary. The front associated with the SAC is indicated as SAF here based on Ueno and Yasuda (2000) and Yasuda (2003)

we have also created a table of metrics that summarizes the basic dynamical properties of each front. We believe that such a table will be helpful for discussing common and unique aspects of oceanic fronts around Japan and serves as a benchmark for examining how well these fronts are represented by numerical models.

This article is organized as follows. In Sect. 2, we introduce the dynamical parameters (i.e., metrics) that are commonly used to describe oceanic fronts and present a table of metrics for the oceanic fronts in the above-mentioned western North Pacific. In Sect. 3, we review the individual fronts in more detail and use the metric table for

comparison, starting from those fronts associated with the Kuroshio. Extra emphasis is placed on the KE since this feature is by far the most well-studied front in the region. Fronts within the KOC region, such as the northern branch of the KE [referred to as the Kuroshio Extension northern branch (KENB) hereafter; see Sect. 4 for details on the terminology] and those in the Subarctic Frontal Zone (SAFZ), are reviewed in Sect. 4. Fronts in the subtropical region are reviewed in Sect. 5. Fronts in the coastal and marginal seas surrounding Japan are reviewed in Sect. 6. The summary and discussion are presented in Sect. 7.

2 A table of metrics

2.1 The dynamical properties of oceanic fronts

What are oceanic fronts? As mentioned earlier, Cromwell and Reid (1956) define an oceanic front as "a band along the sea surface across which the density changes abruptly." Yanagi (1987) defines fronts as "where two water masses meet, with the spatial gradients of temperature and/or salinity much stronger than the background." Since the temperature and salinity of seawater are spatially inhomogeneous in nature, convergence, divergence, shear, and mixing often lead to formation of "fronts" in various places and with different magnitudes. As the mechanism behind the formation of fronts varies, the appropriate set of parameters that describe the underlying dynamics of fronts is also likely to differ for each front. Yanagi (1987) has attempted to classify the oceanic fronts based on their primary forcing agents and geographical locations. In this article, our focus is placed on the dynamical features that are common to many fronts. Our focus is also placed on the fronts' climatological surface properties since the fronts are now recognized as regions of intensive air-sea interaction. For example, the cross-frontal SST gradient is in direct contact with the atmosphere and therefore is emphasized here more than the corresponding gradient in subsurface temperature.

The metrics estimated for individual fronts may be classified into four property types as follows. (1) Geometric properties: the location and length of the oceanic front. The latter metric provides the length scale of the front, which will be important for considering the spatial scale of its dynamics as well as the atmospheric processes it might influence. (2) Surface water mass properties: SST, sea surface salinity (SSS), and their gradients. These metrics are the surface properties of what is traditionally used for defining oceanic fronts and show the differences between the two water masses in contact at the frontal axis. The SST and its gradient are also important parameters on which the heat and moisture exchange with the atmosphere depends. (3) Dynamical properties: sea surface height (SSH) gradient, along-front flow speed, volume transport, frontal depth from the surface, and eddy kinetic energy (EKE) at the surface. These metrics provide the information on the momentum field associated with fronts. The first four of the metrics of dynamical properties describe the mean flow field, while the last one gives a measure of eddy activity. Through the thermal wind balance, cross-frontal density gradients determined from the temperature and salinity distribution are linked to vertical shear in velocity with flow speed typically stronger toward the surface. From the geostrophic balance, the SSH gradient is a surface parameter that reflects the geostrophic velocity at the surface, and the SSH contours are often used for locating the frontal axis. (4) Surface fluxes: latent and sensible heat fluxes. As these are involved in air–sea interaction in the vicinity of an oceanic front, the turbulent heat fluxes depend on both oceanic and atmospheric conditions. The metrics listed above are limited and by no means complete. Although inclusion of some other metrics may lead to a more complete description of frontal characteristics, we focus on the metrics listed above for conciseness. Specific descriptions for individual fronts are given in Sects. 3–6.

2.2 The metric table

Tables 1, 2, 3, 4, and 5 show various metrics estimated at the oceanic fronts. Tables 1, 3, and 4 show the KE, Kuroshio south of Japan (K-SOJ), Kuroshio along the shelf break of the East China Sea (K-ECS), KENB, which is also referred to as the Kuroshio Bifurcation front or the Kuroshio northern branch (see Sect. 4 for details on the terminology), Subarctic Current (SAC), Isoguchi Jets (J1 and J2), SAFZ, and northern, southern, and eastern STFs (Fig. 2). These fronts are associated with the western boundary currents and their extensions or those that form in the interior of the ocean. In addition, the corresponding metrics of fronts in coastal and marginal seas around Japan are presented, such as the tidal fronts of Seto Inland Sea and the Japan Sea subpolar front (JS-SPF) (Table 5). Some fronts that are not located in the western North Pacific are also discussed, mainly for comparison. Specifically, major fronts along the Gulf Stream (GS), Agulhas Current (AC), Agulhas Return Current (ARC), and Antarctic Circumpolar Current (ACC) are compared to the KE (Table 2). Likewise, the Hawaiian Lee Countercurrent (HLCC) is compared to the western Pacific STFs (Table 4).

An overview of the data sets and methods used to estimate the metrics for the aforementioned fronts are given here. More details are described in the Appendix. We made an effort to use similar observational data sets and periods unless noted otherwise (Table 6 in the Appendix), and these data sets are chosen primarily because of the high spatial resolution necessary for representing realistic values for

Table 1 Metrics for the fronts associated with main branch of the Kuroshio: KE, Kuroshio south of Japan, and Kuroshio along the shelf break of the East China Sea

	Kuroshio			
	Extension (observations)	Extension (FRA-JCOPE2)	South of Japan	East China Sea
Acronym	KE	KE	K-SOJ	K-ECS
Location				
Start (lat, lon)	35°N, 141°E	35°N, 141°E	30°N, 131°E	26°N, 124°E
End (lat, lon)	34°N, 165°E	34°N, 165°E	32–34.3°N, 140°E	31°N, 127°E
Length (km)	3000–4000	3000–4000	1000–1500	600
Surface water				
Temperature (°C)	26.8 ± 0.7 [27.2 ± 0.7] (Aug) 16.3 ± 0.6 [16.6 ± 0.8] (Mar)	26.3 ± 0.6 (Sep) [26.7 ± 0.7 (Aug)] 15.8 ± 1.0 (Mar) [16.3 ± 1.1 (Mar)]	28.5 ± 0.26 (Aug) 19 ± 0.39 (Feb)	29.10 ± 0.76 (July) 22.62 ± 0.58 (Jan)
SST gradient [°C (100 km)$^{-1}$]	1.8 ± 0.7 (Dec) [2.1 ± 0.7] (Dec) 0.7 ± 0.2 (Aug) [0.9 ± 0.3] (Aug)	2.4 ± 0.6 (Feb) [2.9 ± 0.8 (Jan)] 0.8 ± 0.2 (Aug) [1.0 ± 0.4 (Aug)]	5 ± 0.80 (Dec) 2.2 ± 0.55 (Aug)	3.63 ± 1.67 (Jan) 0.67 ± 0.97 (July)
Salinity	[34.6] (Apr) [34.2] (Aug)	34.7 ± 0.05 (Apr) [34.7 ± 0.05 (Apr)] 34.3 ± 0.05 (Sep) [34.2 ± 0.06 (Aug)]	34.7–34.8 (Mar) 34–34.1 (Sep)	34.70 ± 0.11 (Jan) 34.12 ± 0.32 (July)
Salinity gradient [(100 km)$^{-1}$]	[0.19] (Sep) [0.10] (May)	0.17 ± 0.04 (Oct) [0.24 ± 0.09 (Oct)] 0.10 ± 0.04 (July) [0.13 ± 0.07(July)]	0.1–0.2 (Sep) 0.02–0.05 (Mar)	1.12 ± 0.95 (July) 0.04 ± 0.11 (Jan)
Dynamics				
SSH gradient [cm (100 km)$^{-1}$]	61 ± 11 [71 ± 13] (Ann)	52 ± 12 [61 ± 16] (Ann)	80 ± 2.9 (Ann)	50 ± 4 (Ann)
Flow speed (m s^{-1})	*1.4*	1.0 ± 0.3 (10 m) (Ann)	*0.70–1.5*	*1*
Transport (Sv)	*140*		*42*	*25*
Depth (m)	*500–1500*		*1000*	*700*
EKE (m^2 s^{-2})	*0.09*		0.05–0.2	*0.1*
Heat flux				
Latent flux (W m^{-2})	260 ± 37 [290 ± 45] (Dec) 30 ± 12 [30 ± 15] (July)	Net flux 440 ± 40 [500 ± 50] (Jan) 80 ± 20 [90 ± 20] (July)	290 ± 41 (Dec) 55 ± 12 (June)	278 ± 34 (Dec) 75 ± 13 (June)
Sensible flux (W m^{-2})	110 ± 13 [140 ± 18] (Jan) 0 ± 3 [10 ± 5] (Aug)		140 ± 16 (Jan) 5 ± 3 (July)	106 ± 12 (Jan) 2 ± 2 (July)

The metrics for KE are provided from observations (left) and FRA-JCOPE2 (right). The acronyms of the fronts are written in the first row. The metrics are categorized into four property types, which are written in the first column. Those with two rows show the maximum monthly mean above the minimum monthly mean with the months written in brackets. Annual means are indicated as Ann. The magnitude of the interannual variability is shown with the ± signs. Metrics for KE show values from the whole frontal axis and those from the upstream axis in [squared brackets]. Metrics from past studies are written in *italics* and those from numerical models are underlined. Detailed methods about how each metric is estimated are provided in the Appendix

Table 2 Metrics for major fronts compared to the KE: the Gulf Stream, Agulhas Current, Agulhas Return Current, and Antarctic Circumpolar Current-Subantarctic front

	Gulf Stream	Agulhas Current	Agulhas Return Current	Antarctic Circumpolar Current-Subantarctic front
Acronym	GS	AC	ARC	ACC-SAF
Location				
Start (lat, lon)	35°N, 75°W	27°S, 33°E	40°S, 19°E	41°S (north) 0–360°E
End (lat, lon)	40°N, 50°W	40°S, 19°E	45°S, 66°E	60°S (south) 0–360°E
Length (km)	3500	2000	3900	31,000
Surface water				
Temperature (°C)	27 ± 0.8 (Aug) 12 ± 2.5 (Mar)	28 ± 2 (Feb) 19 ± 1 (Aug)	15 ± 2 (Feb) 10 ± 2 (Aug)	8.0 ± 0.7 (Feb) 4.8 ± 0.5 (Sep)
SST gradient [°C (100 km)$^{-1}$]	4 ± 1.5 (Mar)	1.8 ± 0.7 (Ann)	4.1 ± 1.2 (Ann)	0.9 ± 0.1 (Mar) 0.8 ± 0.1 (Aug)
Salinity	35–36 (Ann)	35.5 (Ann)	34.5 (Ann)	34 (Ann)
Salinity gradient [(100 km)$^{-1}$]	0.5 (Ann)	0.1 (Ann)	0.4 (Ann)	0.05 (Ann)
Dynamics				
SSH gradient [cm (100 km)$^{-1}$]	80 ± 30 (Ann)	70 ± 20 (Ann)	50 ± 20 (Ann)	*20–70*
Flow speed (m s^{-1})	*1.5*	*1.2*	*0.8*	*0.4*
Transport (Sv)	*140*	*70*	*54*	*30–60*
Depth (m)	*3500*	*2400*	*1500*	*2500*
EKE (m^2 s^{-2})	0.2 ± 0.1 (Ann)	0.1 ± 0.1 (Ann)	0.2 ± 0.2 (Ann)	*0.4*
Heat flux				
Latent flux (W m^{-2})	350 ± 75 (Jan) 100 ± 25 (July)	327 ± 67 (Aug) 191 ± 30 (Jan)	251 ± 31 (Aug) 181 ± 34 (Jan)	65 ± 7 (Sep) −39 ± 4 (Jan)
Sensible flux (W m^{-2})	150 ± 45 (Jan) 10 ± 5 (July)	111 ± 34 (July) 56 ± 11 (Jan)	71 ± 21 (July) 38 ± 11 (Feb)	3.0 ± 3.5 (Sep) −7.5 ± 2.0 (Feb)

See the footnote of Table 1 for descriptions

sharp gradients of oceanic variables and thus for defining fronts. For the surface water mass properties in Tables 1, 2, 3, 4, and 5, monthly means of AMSR-E SST (2003–2008; Gentemann et al. 2010), MGDSST (2003–2008; Kurihara et al. 2000), and OISST (2003–2008; Reynolds et al. 2002, 2007) are used for estimating the SST and its gradient. The monthly climatology of World Ocean Atlas 2005 (Antonov et al. 2006), 2009 (Antonov et al. 2010), and 2013 (Zweng et al. 2013) is used for estimating the SSS and its gradient. For the dynamical properties, the monthly mean of AVISO (1993–2007; http://www.aviso.oceanobs.com/duacs/) is used for estimating the SSH gradient and EKE. The EKE is based on geostrophic velocity anomalies. For the surface fluxes, monthly means of latent heat and sensible heat fluxes are obtained from Version 2 of Japanese Ocean Flux data sets using Remote Sensing Observations (J-OFURO2; 1993–2007; Tomita et al. 2010). The J-OFURO2 is chosen because of its best estimate for the KE region (Tomita et al. 2010). Standard deviation of the interannual variability is provided for SST, SSH, their gradients, EKE, and the heat fluxes so that they provide a measure of the variability observed at the fronts. However, SSS and its gradient are only presented with their monthly means because only the climatological monthly means are available and interannual variability cannot be estimated. Other metrics, such as location, along-front flow speed, volume transport, and frontal depth, are mostly based on past studies. Metrics are also estimated from Japan Coastal Ocean Predictability Experiment-2 (JCOPE-2; Miyazawa et al. 2009; see Appendix) for the KE (Table 1). This is to compare how well current state-of-the-art data assimilation models capture the observed frontal signatures.

The estimates of each metric are based on monthly mean fields unless noted otherwise. This is because we aim to present a climatological view of oceanic fronts and many of the past studies are based on monthly means. Many fronts are also highly variable in time, and we find it reasonable to focus on the monthly mean time scale to distinguish the role of fronts from eddies with much smaller time scales. Spatial gradients are per 100 km instead of estimating their local maximum. We chose to use this spatial scale because it can roughly present the difference in the values across a front and is the spatial scale at which the atmosphere is likely to be affected. A higher spatial scale can capture the

Table 3 Metrics for fronts within the Kuroshio-Oyashio confluence region: the Kuroshio Extension northern branch, Subarctic Current, Isoguchi Jets (J1 and J2), and Subarctic Frontal Zone

	Kuroshio Extension northern branch	Subarctic Current	Isoguchi Jets		Subarctic Frontal Zone
			J1	J2	
Acronym	KENB	SAC	J1	J2	SAFZ
Location					
Start (lat, lon)	38°N, 153°E	41°N, 150°E	40°N, 150°E	40°N, 165°E	40°N, 145°E
End (lat, lon)	40°N, 170°E	44°N, 155°E	43°N, 155°E	43°N, 170°E	45°N, 180°
Length (km)	2000	500	500	500	6000
Surface water					
Temperature (°C)	22.3 ± 0.7 (Sep) 11.2 ± 0.2 (Mar)	18.1 ± 0.7 (Aug) 4.0 ± 0.5 (Apr)	19.9 ± 0.8 (Aug) 7.0 ± 0.4 (Mar)	18.8 ± 1.2 (Sep) 7.8 ± 0.4 (Mar)	17 ± 1.0 (Sep) 5.6 ± 0.2 (Mar)
SST gradient [°C (100 km)$^{-1}$]	1.9 ± 0.4 (June) 0.7 ± 1.0 (Nov)	3.3 ± 0.4 (Apr) 2.0 ± 1.5 (Oct)	3.6 ± 0.8 (Jan) 0.6 ± 0.9 (July)	3.6 ± 0.6 (Feb) 2.0 ± 0.4 (Sep)	
Salinity	34.4 (May) 34.2 (Aug)	33.6 (Mar) 33.1 (Sep)	33.9 (Mar) 33.5 (Dec)	33.9 (June) 33.6 (Aug)	33.0–33.9 (Ann)
Salinity gradient [(100 km)$^{-1}$]	0.11 (Ann)	0.54 (Sep) 0.35 (Apr, Dec)	0.50 (Dec) 0.34 (Mar)	0.47 (Nov) 0.32 (Feb)	0.2 (Ann)
Dynamics					
SSH gradient [cm (100 km)$^{-1}$]	5.2 ± 13.0 (Ann)	12.9 ± 6.9 (Ann)	19.0 ± 4.7 (Ann)	14.2 ± 4.8 (Ann)	
Flow speed (m s^{-1})	0.05 ± 0.14 (Ann)	0.13 ± 0.07 (Ann)	0.19 ± 0.05 (Ann)	0.14 ± 0.05 (Ann)	
Transport (Sv)	15* (0–1500 m)	*10*	10* (0–1500 m)	10* (0–1500 m)	
Depth (m)	300	300	300	300	
EKE (m^2 s^{-2})	0.021 ± 0.007 (Ann)	0.008 ± 0.004 (Ann)	0.013 ± 0.006 (Ann)	0.009 ± 0.005 (Ann)	
Heat flux					
Latent flux (W m^{-2})	209 ± 29 (Dec) 2 ± 12 (July)	119 ± 20 (Dec) −21 ± 11 (July)	163 ± 26 (Dec) −12 ± 15 (July)	156 ± 25 (Dec) −12 ± 11 (July)	136 ± 20 (Dec) −17 ± 9 (July)
Sensible flux (W m^{-2})	81 ± 10 (Jan) −1 ± 3 (July)	54 ± 16 (Dec) −12 ± 5 (May)	89 ± 12 (Jan) −3 ± 7 (May)	49 ± 16 (Dec) −6 ± 3 (July)	49 ± 15 (Dec) −9 ± 3 (May)

Metrics noted with asterisks are our rough estimates (see Appendix). See the footnote of Table 1 for further descriptions

abrupt changes at the front better, but is likely to result in large uncertainties as well. We also tried to avoid the differences that arise from products with a different spatial resolution because high spatial resolution products tend to resolve gradients better and thus yield stronger local maxima of gradient intensity. The metrics are provided with monthly maximum and minimum values to present the climatological seasonal cycle, and the variability on a shorter or longer time scale is described in Sects. 3–6 where necessary.

3 Kuroshio fronts

3.1 Kuroshio Extension front (KE front)

The Kuroshio separates from the Japanese coast at the Boso Peninsula at around 35°N, forming an eastward jet known as the KE (Fig. 2). This jet is accompanied by two prominent meanders between the Izu Ridge and the Shatsky Rise (e.g., Fig. 2 of Niiler et al. 2003a). The jet is also accompanied by a sharp subsurface density front, known as the KE front, characterized by a steep upward slope of the main pycnocline tilting northward. Since the subtropical main pycnocline is controlled by the temperature stratification, the KE front is essentially a temperature front (Fig. 2 of Nonaka et al. 2006). The position of the KE front is known to differ from the subtropical-subpolar boundary that is predicted from the Sverdrup streamfunction in the interior. The northern recirculation gyre to the north of the KE (Qiu et al. 2008; Nakano et al. 2008) and effects of eddies (e.g., Waterman et al. 2011) may contribute to this discrepancy between the Sverdrup streamfunction and the observed KE front. Despite the many studies carried out thus far, we have not reached a full understanding of how the KE front forms and how its mean position is determined.

3.1.1 Metrics used to locate the KE front

The importance of the KE for fisheries led to the early establishment of metrics that have been used operationally

Table 4 Metrics for fronts located in the subtropical gyre of the North Pacific: Northern, Southern, and Eastern subtropical fronts and the Hawaiian Lee Counter Current

	Subtropical front			Hawaiian Lee Countercurrent
	North	South	East	
Acronym	NSTF	SSTF	ESTF	HLCC
Location				
Start (lat, lon)	22–25°N, 130°E	18–20°N, 130°E	25–27°N, 180°	18°N, 165°E
End (lat, lon)	22–25°N, 180°	21–22°N, 180°	25–27°N, 140°W	19–20°N, 160°W
Length (km)	5100	5200	4000	7000
Surface water				
Temperature (°C)	29 ± 0.4 (July–Sep) 24 ± 0.3 (Feb–Mar)	29 ± 0.3 (July–Sep) 27 ± 0.3 (Feb–Mar)	27 ± 0.3 (Aug–Sep) 22 ± 0.6 (Feb–Mar)	28 ± 0.2 (Sep) 25 ± 0.2 (Feb)
SST gradient [°C (100 km)$^{-1}$]	0.7 ± 0.1 (Feb–Mar) 0.2 ± 0.1 (Aug– Oct)	0.3 ± 0.1(Jan–Feb) 0.1 ± 0.04 (July–Aug)	0.7 ± 0.1 (Feb–Mar) 0.2 ± 0.1 (July–Sep)	
Salinity	35.1 (Jan–July) 34.9 (Sep)	34.9 (Jan–July) 34.7 (Sep)	35.4 (July–Aug) 35.2 (Mar)	34.9 (Sep–Jan) 34.7 (May)
Salinity gradient [(100 km)$^{-1}$]	0.03 (Ann)	0.06 (Ann)	0.03 (Ann)	0.06 (Ann)
Dynamics				
SSH gradient [cm (100 km)$^{-1}$]	4 ± 4 (May) 0.4 ± 3 (Sep–Nov)	3 ± 4 (Mar–Apr) 0.4 ± 2 (Nov–Dec)	4 ± 3 (Ann)	3.3 ± 2.9 (Ann)
Flow speed (m s^{-1})	0.08 ± 0.06 (May) 0.01 ± 0.06 (Sep–Nov)	0.05 ± 0.08 (Mar–Apr) 0.01 ± 0.05 (Nov–Dev)	0.05 ± 0.05 (Ann)	0.11 + 0.05 (Oct) 0.05 ± 0.04 (Mar)
Transport (Sv)				4.4
Depth (m)				180
EKE (m^{2}s^{-2})	0.031 ± 0.006 (May–June) 0.017 ± 0.003 (Dec–Jan)	0.035 ± 0.009 (May) 0.018 ± 0.005 (Dec–Jan)	0.017 ± 0.005 (Apr–June) 0.012 ± 0.003 (Nov–Jan)	*0.022 ± 0.036 (Ann)*
Heat fluxes				
Latent flux (W m^{-2})	160 ± 20 (Nov–Jan) 90 ± 20 (May–June)	180 ± 20 (Nov–Dec) 110 ± 10 (June–Aug)	160 ± 20 (Nov–Jan) 100 ± 20 (May–June)	195 ± 23 (Dec) 124 ± 21 (May)
Sensible flux (W m^{-2})	20 ± 4 (Jan–Feb) 2 ± 2 (Aug–Sep)	10 ± 4 (Jan–Feb) 3 ± 2 (Apr–Nov)	12 ± 5 (Nov–Mar) 4 ± 2 (June–Aug)	13 ± 4(Mar) 4 ± 1(July)

See the footnote of Table 1 for descriptions

for detecting the KE axis. While the position of the KE axis is ideally defined from the maximum velocity at the surface, it was traditionally based on subsurface temperature. This is because temperature data are more commonly available, and there is a close relationship between the subsurface density/temperature front and the velocity structure of the KE. Kawai (1969, 1972) suggested that the position of the maximum surface velocity across the KE is well correlated with the positions of the following isotherms: 13.9 and 13.7 °C at a depth of 200 m in the longitudinal sectors from 143.5°E to 145.5°E and from 148.0°E to 151.5°E, respectively (Fig. 3); 9.0 and 8.0 °C at a depth of 400 m are also used for the two sectors. These metrics are based on a statistical analysis of quasi-concurrent synoptic measurements of subsurface temperature and surface velocity. The 14.0 °C isotherm at 200 m has been widely used as a metric for locating the KE axis but, at times, beyond the domains examined by Kawai (e.g., Bingham 1992). This is likely because the availability of temperature data is higher at 200 m depth than at 400 m depth although the 9 °C isotherm at 400 m depth corresponds better to the KE axis. Another widely used metric was that proposed by Mizuno and White (1983), who found that the location of the 12 °C isotherm at 300 m depth as a metric is well suited for locating the KE axis based on 1° latitude/longitude gridded seasonal-mean temperature fields. There appears to be a high correlation between 300 m temperature and dynamic thickness between 100 and 1000 db in the mid-latitude western North Pacific at least as far east as 170°E (Bernstein and White 1981) in all seasons. The 12 °C isotherm at 300 m depth is also widely accepted as a metric for the KE axis (e.g., Suga et al. 1997). Murakami (1993) proposed a metric for the KE axis with an indicative temperature at 100 m depth. The depth, however, may

Table 5 Metrics for fronts located in the coastal and marginal seas around Japan: Seto Inland Sea tidal front and Japan Sea subpolar front

	Seto Inland Sea tidal front	Japan Sea subpolar front
Acronym		JS-SPF
Location		
Start (lat, lon)	33.24°N, 131.85°E	40°N, 133°E
End (lat, lon)	33.38°N, 132.08°E	40°N,138°E
Length (km)	40	400
Surface water		
Temperature (°C)	*23*	23.7 ± 1.1 (Aug) 6 ± 1.1 (Mar)
SST gradient [°C (100 km)$^{-1}$]	*4 °C/10 km*	4.2 ± 0.6 (Jan) 1.3 ± 0.3 (Aug)
Salinity	*34*	34.1 (Jan–May) 33.6 (Oct–Nov)
Salinity gradient [(100 km)$^{-1}$]	*0.6/10 km*	0.18 (Oct) −0.13 (June)
Dynamics		
SSH gradient [cm (100 km)$^{-1}$]	*1.0 cm/10 km*	11.3 ± 1.5 (Ann)
Flow speed (m s^{-1})	*0.1–0.2*	*0.3*
Transport (Sv)	*0.01*	*1.2*
Depth (m)	*20*	*200*
EKE (m^2 s^{-2})	*0.01–0.04*	
Heat fluxes		
Latent flux (W m^{-2})	120 (Nov) 40 (June–July)	169 ± 26 (Dec) −6 ± 11 (July)
Sensible flux (W m^{-2})	20 (Dec) 0 (July–Aug)	107 ± 31 (Dec) −4 ± 4 (May)

The gradients for the Seto Inland Sea are per 10 km since its spatial scale is <100 km. See the footnote of Table 1 for descriptions

be too shallow to apply throughout the year since the KE axis shows distinct seasonality in its best correspondence to a particular isotherm, which varies from 16 °C in February to 19 °C in October.

Representation of the mean state and variability of the KE has been revolutionized by the advent of satellite altimetry (e.g., Qiu et al. 1991). With gridded products of SSH, one can define the KE path by tracing an appropriate SSH contour that is located along or in the immediate vicinity of local SSH gradient maxima (e.g., Qiu and Chen 2005; Sugimoto and Hanawa 2012). As an example, Qiu and Chen (2005) offered a comprehensive description of the position and length of the KE path, cross-frontal SSH gradient, and EKE within the KE region, in addition to their decadal variability (Table 1). Note that the absolute values of SSH used as an indicator of the KE path depend on a particular SSH product because the global mean SSH values are different between the SSH products.

Figure 3 shows the locations of the KE axis as defined by the isotherms of 14 °C at 200 m depth (red), 12 °C at 300 m depth (blue), and 9 °C at 400 m depth (green), in addition to the axis defined as the contour line of SSH (=0.05 m) (black), all of which are based on the 1993–2007 annual climatology derived from the FRA-JCOPE2 reanalysis (Miyazawa et al. 2009). It is evident that all the metrics correspond well to the core of the surface velocity (shading) in the FRA-JCOPE2 reanalysis, especially near Japan, although their discrepancy increases rapidly downstream. Miyazawa et al. (2009) pointed out that variations of the KE as defined by tracking grid points of maximum kinetic energy at 100 m depth of the JCOPE2 reanalysis compare well with the observational counterpart, including decadal variability of the KE. Consistency among the definitions of the KE path can also be confirmed in climatological maps based on observations (Fig. 4) where the two isotherms of 14 °C at 200 m depth and 12 °C at 300 m depth roughly correspond to the large SSH gradient associated with the KE at 141°E–165°E. While more rigorous comparison between the indicative isotherms and their SSH counterpart may be needed for more in-depth discussions, all of the aforementioned metrics used for determining the KE axis seem appropriate.

3.1.2 The KE front and its impact on the atmosphere

The flow field associated with the KE can be divided into up- and downstream regions by the 153°E meridian according to the satellite observations (e.g., Qiu and Chen 2005). The KE in the upstream region (west of 153°E) is characterized by the presence of two quasi-stationary meanders, whereas the KE in the downstream region (153°E–165°E) bifurcates into the (main) KE and the northern branch (KENB). The magnitude of the SST gradient associated with the KE exhibits a clear seasonality with the maximum in winter [about 2 °C (100 km)$^{-1}$] and minimum in summer [about 1 °C (100 km)$^{-1}$] (Table 1; Fig. 5). In the upstream region, the strengths of the SST and SSH gradients, in addition to the flow speed, exhibit seasonal (Tatebe and Yasuda 2001) and interannual to decadal variability (Qiu and Chen 2005, 2010a); therefore, the "typical" values listed in Table 1 include some uncertainty. It is argued (e.g., Howe et al. 2009) that the KE may be better captured in the stream-coordinate system, in which no lateral smoothing of the jet structure can occur that arises from the Eulerian mean of the highly variable KE axis. Our estimates for the SST, SSH, and their gradients are therefore based on the stream-coordinate system. As evident in Fig. 5, the SST gradient associated with the KE in its upstream region based on FRA-JCOPE2 reanalysis exhibits large interannual variations, whose strength is comparable to that of the climatological seasonal cycle.

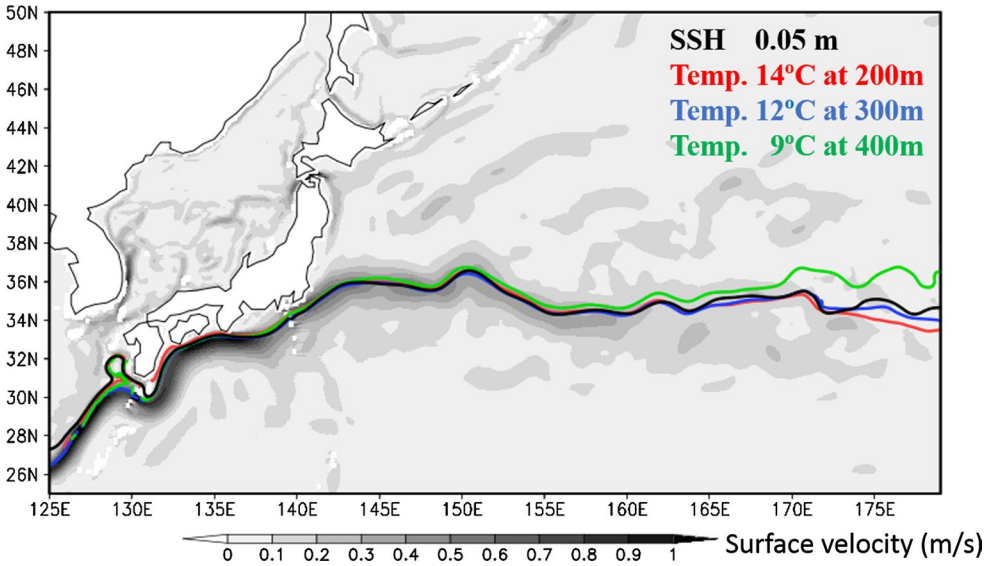

Fig. 3 Comparison of the locations of the KE calculated from the annual mean 1993–2007 climatology of the FRA-JCOPE2 reanalysis. Isocline contours are 14 °C at 200 m depth (*red*), 12 °C at 300 m depth (*blue*), and 9 °C at 400 m depth (*green*) of the potential temperatures and 0.05 m of the sea surface height (*black*). *Gray shading* shows the surface absolute velocity at 10 m depth

While the KE is associated with a thermocline front, it transports warm water and causes a strong SST front just to the north of its axis, especially in winter (Fig. 4). Along this SST front, turbulent surface heat fluxes also exhibit a strong frontal gradient (Fig. 4e, f), especially in the KE upstream region (Figs. 2 and 3 of Taguchi et al. 2009). At 145°E, for example, the meridional SST gradient exceeds 6 °C (100 km)$^{-1}$ in winter, while the corresponding gradient in the turbulent heat flux (sum of latent and sensible heat fluxes) reaches as high as 100 W m^{-2} (100 km)$^{-1}$. Along the warm KE, latent heat flux is locally enhanced particularly in winter, supplying moisture to the atmosphere (e.g., Iizuka 2010), which is numerically found to be important for cyclone intensification (Iizuka et al. 2013). Observations and numerical models both show that sensible heat flux is also enhanced along the KE axis in winter, which leads to the climatological formation of a near-surface pressure trough slightly south of the KE (Tanimoto et al. 2011) and associated local maxima of cloudiness (Tokinaga et al. 2009; Masunaga et al. 2014). Observations also reveal changes in the SST and turbulent heat flux (sum of latent and sensible heat fluxes), which reflect the changes in the KE path. The KE front shows a decadal-scale north-south movement ranging approximately 200 km in latitude (Qiu and Chen 2005, 2010a), which yields large SST anomalies persistently between 34° and 36°N exerting significant synoptic-scale changes in PBL (Joyce et al. 2009). Additionally, the KE front alternates decadally between a stable state with two quasi-stationary meanders and an unstable state with a convoluted path (Qiu and Chen 2005; Seo et al. 2014a); in the unstable state, warm eddies detach northward from the KE front (Itoh and Yasuda 2010), resulting in increased SST and upward heat release in winter (Sugimoto and Hanawa 2011).

In summer, by contrast, meridional gradients of SST and turbulent heat flux at 145°E drop to about 2 °C (100 km)$^{-1}$ and 20 W m^{-2} (100 km)$^{-1}$, respectively (Fig. 4d), although the flow speed as derived from the SSH gradient exhibits no significant seasonality (Table 1). In situ observations by Tanimoto et al. (2009) revealed distinct impacts of the KE on summertime low-level clouds. Fog formation is likely over the cooler water with the warm, moist southerly winds across the KE, whereas the formation of convective stratocumulus is most likely over the warm KE under the cool northerlies. This tendency of low-level clouds is confirmed by another in situ observation by Kawai et al. (2014), who also show that the depth of the PBL is modulated in the presence of the KE especially in its upstream region. They nevertheless observed a local minimum of relative humidity over the warm KE, along which turbulent activity within the PBL and the consequent entrainment of free-tropospheric air into the PBL were both locally enhanced under the cool northerlies.

3.2 Kuroshio south of Japan

The Kuroshio is observed to flow into the deep Shikoku Basin from the shallow East China Sea through the Tokara Strait (Fig. 2). This portion of the Kuroshio within the Shikoku Basin, which we refer to as the K-SOJ, can take different paths: the "straight path" and "large meander path" (Kawabe 1995). The path length of the Kuroshio axis between 131°E and 140°E is about 1,000 and 1,500 km for the straight and large-meander paths, respectively (Table 1), which are estimated by tracking the strongest part of the surface geostrophic current (Ambe et al. 2004). These two states persist from a year to a decade (Kawabe 1987). Recent modeling studies indicate that the large meander

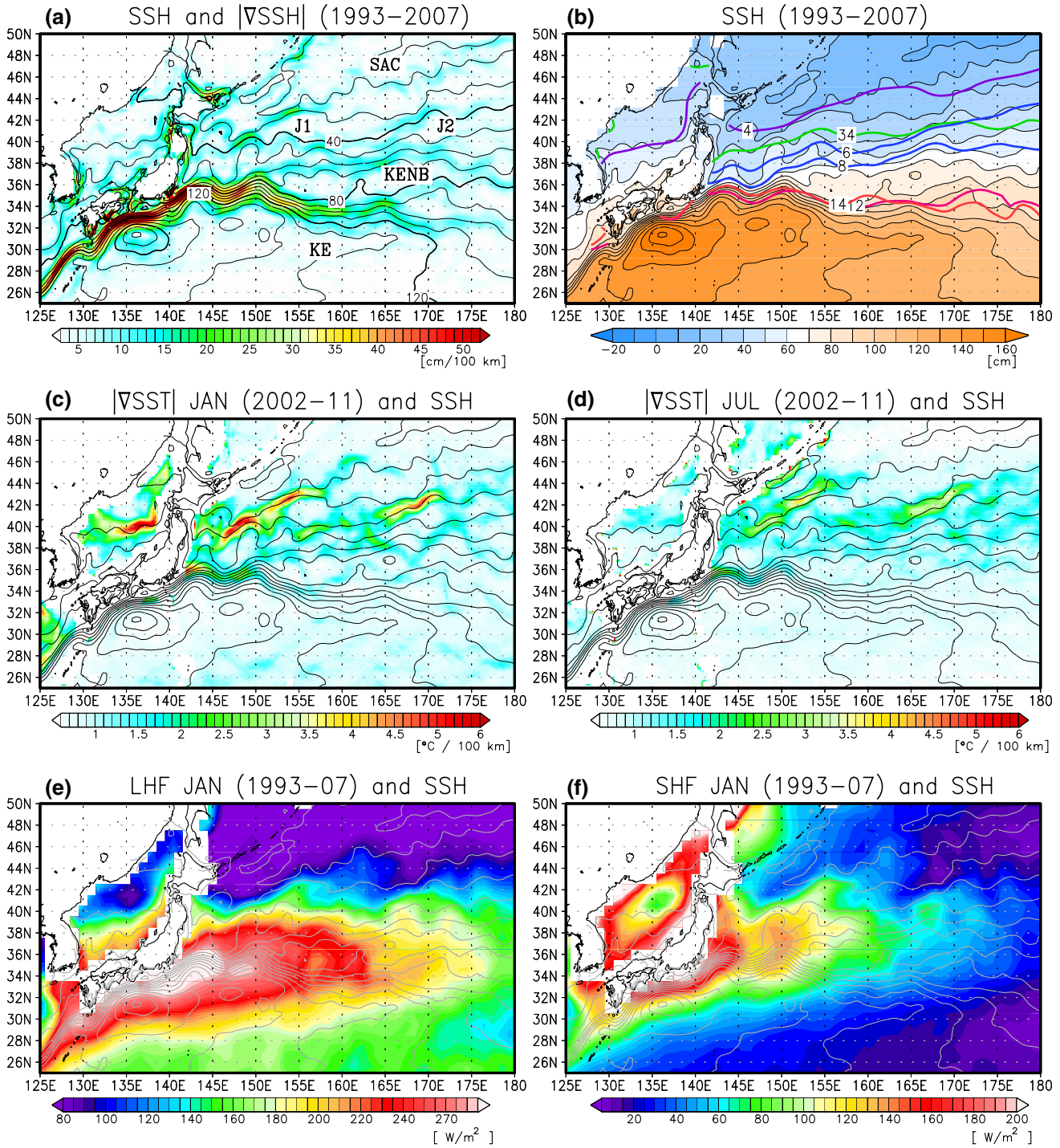

Fig. 4 **a** Annual climatology (1993–2007) of SSH (contoured every 10 cm) and its horizontal gradient [cm (100 km)$^{-1}$; *shaded*] based on AVISO (Rio et al. 2011). **b** The corresponding climatological SSH (contoured every 10 cm) and the following associated fronts and jets: (*red line*) KE defined by the 14 °C isotherm at 200 m depth (Kawai 1972); (*magenta line*) KE defined by the 12 °C isotherm at 300 m depth (Mizuno and White 1983); (*blue lines*) KENB defined by the 6 and 8 °C isotherms at 300 m depth (Mizuno and White 1983); (*green line*) subarctic boundary defined by the salinity of 34.0 at 100 m depth (Favorite et al. 1976); (*purple line*) SAC traced by the 4 °C isotherm, which is the southern boundary of the "pure" subarctic water (Favorite et al. 1976; Belkin et al. 2002). Temperature and salinity are based on WOCE Global Hydrographic Climatology (Gouretski and Koltermann 2004). **c** The horizontal gradient of SST in January [°C (100 km)$^{-1}$; *shaded*] based on the January climatology (September 2002–August 2011) of AMSR-E SST. Annual climatology of SSH (same as **a**) is contoured every 10 cm. **d** Same as **c** but for July. **e** January climatology of latent heat flux (W m^{-2}; *shaded*) based on the J-OFURO2 (1993–2007). Annual climatology of SSH (same as **a**) is contoured every 10 cm. **f** Same as **e** but for sensible heat flux

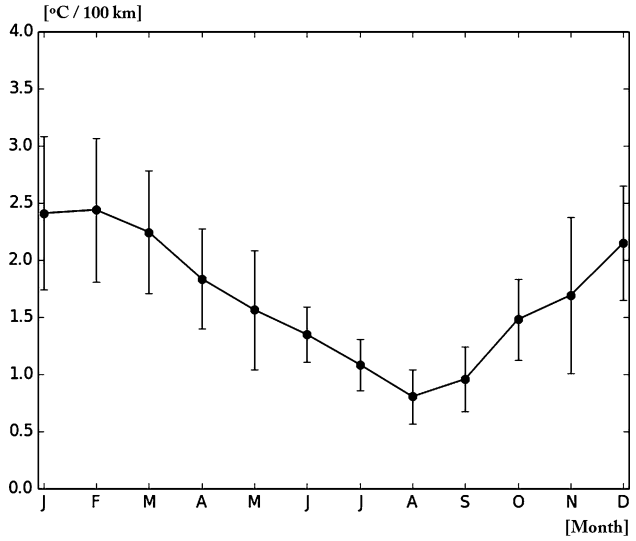

Fig. 5 Seasonal variations of SST gradient [°C (100 km)$^{-1}$; *dots*] across the KE between 141°E and 165°E based on the monthly climatology (1993–2007) of the FRA-JCOPE2 reanalysis data. Maximum and minimum values are those presented in Table 1. The interannual standard deviation of the SST gradient is indicated as a *bar* for each calendar month

tends to occur and persist when the volume transport is low (Tsujino et al. 2013; Usui et al. 2013).

The velocity of the Kuroshio has a subsurface maximum and extends downward to at least 1,000 m (Table 1, e.g., Nakano et al. 1994; Book et al. 2002). Due to its deep structure, the Kuroshio is accompanied by a large SSH gradient across its axis [80 cm (100 km)$^{-1}$] (Fig. 4a). The annual mean volume transport of the Kuroshio is 42 Sv (Imawaki et al. 2001), which almost corresponds to the wind-driven Sverdrup transport. The seasonal variation of the transport (about 10 Sv) is, however, much less than that expected from the Sverdrup transport because of the existence of the Izu-Ogasawara Ridge, which, based on a numerical model, filters the seasonal signal propagating westward from the interior (Isobe and Imawaki 2002).

In contrast to the velocity-related variables, surface temperature and salinity exhibit significant seasonal changes (Table 1). In SST fields, the Kuroshio can be recognized as a warm tongue (e.g., Shimada et al. 2005). The particular feature emerges distinctly in winter and diminishes in summer. As a result, a strong SST front [5 °C (100 km)$^{-1}$] is formed in winter between the warm tongue and relatively cold coastal waters to the north of the Kuroshio (Fig. 4c), while it weakens in summer [2.2 °C (100 km)$^{-1}$] (Fig. 4d). It is well known that the 15 °C isotherm at 200 m depth is a good indicator for the Kuroshio axis (Kawai 1969), but it is usually difficult to define a specific value of SST that corresponds to the Kuroshio axis because of the strong seasonal change in SST. A salinity front is also formed between offshore high-salinity water of the Kuroshio and nearshore low-salinity water because of river discharge (Imasato and Qiu 1987). Unlike the SST front, the magnitude of the salinity front is at its maximum [0.1–0.2 (100 km)$^{-1}$] in summer and minimum in winter [0.02–0.05 (100 km)$^{-1}$].

Surface latent and sensible heat fluxes in the region south of Japan also undergo substantial seasonal variations (Kubota et al. 2002). Under the winter monsoon, outbreaks of cold and dry continental air over the persistently warm surface water of the Kuroshio induce a large amount of heat release from the ocean to the atmosphere (Kwon et al. 2010). In winter, the latent and sensible heat fluxes over the Kuroshio reach 290 and 140 W m^{-2} (Fig. 4e, f), respectively, while they diminish in summer and the sensible heat flux even becomes negative at times. A recent observational study by Nakamura et al. (2012) showed that the huge heat release and bimodal path fluctuations of the Kuroshio have an impact on the development and tracks of wintertime extratropical cyclones passing south of Japan.

3.3 Kuroshio along the shelf break of the East China Sea

The path of the K-ECS is almost fixed and thus much more stable than that to the south of Japan (Fig. 2). The front along the Kuroshio is one of the ten thermal fronts in the East China, Yellow, and Bohai Seas identified from the satellite SST data (HicKox et al. 2000). The Kuroshio front forms between the Kuroshio main current and continental shelf water, extending from the northeast of Taiwan (26°N, 124°E) to the southwest of Kyushu (31°N, 127°E) (HicKox et al. 2000). The Kuroshio surface water is 29 °C in summer and remains warm (22 °C) in winter, while the continental shelf water is 28 °C in summer but cools down to 15 °C in winter under the cold monsoonal airflow because of the shallow bathymetry. Consequently, the Kuroshio front is much stronger in winter than in summer. The maximum water temperature difference across the Kuroshio front is approximately 4 °C in winter but diminishes in summer (HicKox et al. 2000) (Table 1; Fig. 4c, d).

It is difficult to identify a salinity front between the Kuroshio main current and shelf water. An apparent salinity front exists just offshore of the Changjiang River mouth throughout the year (Chen 2009). The low-salinity shelf water and high-salinity Kuroshio surface water maintain the salinity gradient across the Kuroshio main current. The salinity of the Kuroshio surface water is 34.8 in winter and decreases to 34 in summer. Low-salinity water from the river mouth spreading more in summer toward the northern continental shelf enhances the salinity gradient (Chen 2009).

The surface current is strong in summer and weak in winter (Kawabe 1988; Oka and Kawabe 1998). However, the volume transport of the Kuroshio in the East China Sea exhibits only a small range of seasonal variation (4 Sv in Fujiwara 1981; 3.7 Sv in Hinata 1996; 1.6 Sv in Andres et al. 2008) compared to the Sverdrup transport calculated from the basin-scale wind fields (Kagimoto and Yamagata 1997). Observations of the Kuroshio Transport across the PN transect show high-frequency variations as large as 10 Sv, which may be caused by frontal eddies (Ichikawa and Beardsley 1993).

The SST of the Kuroshio exerts influences on the overlying atmosphere (Fig. 4e, f). The winter thermal front across the Kuroshio pathway is observed to weaken the surface winds (Kasamo et al. 2014), and the frontal SST gradient along the shelf break contributes positively to cyclone development (Xie et al. 2002). The high SST along the Kuroshio is also found, from observations and numerical models, to play a critical role in organizing an early summer convective rainband (Miyama et al. 2012), thus forming a local rainfall maximum in June (Sasaki et al. 2012a).

3.4 Comparison to the Gulf Stream, Agulhas Current, and Antarctic Circumpolar Current

To further shed light on the characteristics of oceanic fronts associated with the Kuroshio, it is useful to make a comparison with those associated with the GS, AC, ARC, and ACC. As will be seen in this subsection, these oceanic fronts have similarities in many different aspects with the oceanic fronts associated with the Kuroshio.

The GS is the counterpart of the Kuroshio and the KE in the North Atlantic subtropical gyre. In particular, after the separation at Cape Hatteras, the GS has many similarities to the KE as a free eastward jet associated with strong eddy activity. The GS transports a large amount of warm water poleward, especially in this downstream region (from 60 to 140 Sv between 55°W and 75°W; Johns et al. 1995), and yields a large amount of heat/moisture release into the atmosphere (500 W m^{-2}) (Fig. 1; Table 2). A sharp SST front also extends along its northern flank after the separation at Cape Hatteras [4 °C $(100\ km)^{-1}$ in winter], which is comparable to that of the KE front (Table 1). With this SST gradient and strong land-sea thermal contrasts with the North American continent, the GS exerts a strong influence on the overlying atmosphere (e.g., Minobe et al. 2008, 2010; Kuwano-Yoshida et al. 2010; Nakamura et al. 2004, 2010), as is found for the KE. The large heat release by the GS results in surface wind convergence aloft and plays an important role in the enhanced precipitation over the GS (Minobe et al. 2008; Kuwano-Yoshida et al. 2010).

The AC (Gordon 1985) and ARC (Lutjeharms and Ansorge 2001; Nonaka et al. 2009; Tozuka and Cronin 2014) are the counterparts of Kuroshio and KE in the South Indian Ocean subtropical gyre (Beal et al. 2011) (Fig. 1; Table 2). Large amounts of heat, which are comparable to the Kuroshio and KE, are released into the atmosphere with the maximum latent and sensible fluxes of 327 and 111 W m^{-2}, respectively. We note that these values obtained from the J-OFURO2 data (Tomita et al. 2010) are much larger than 206 and 61 W m^{-2}, respectively, of the OAFlux data (Yu and Weller 2007). The AC and ARC accompany the SST (SSS) gradient of 1.8 °C $(100\ km)^{-1}$ [0.1 $(100\ km)^{-1}$] and 4.1 °C $(100\ km)^{-1}$ [0.4 $(100\ km)^{-1}$], respectively, which are as strong as their counterpart in the KE region. The strong SST gradient is due to large transport by these two currents (Tozuka and Cronin 2014); the mean volume transport of the AC and ARC is estimated to be 70 Sv (Bryden et al. 2005) and 54 Sv (Lutjeharms and Ansorge 2001), respectively. Compared to the K-SOJ, the volume transport of the AC is about 30 Sv stronger. An active ocean-atmosphere interaction occurs over the ARC region (Liu et al. 2007; Nonaka et al. 2009; Tozuka and Cronin 2014), and the associated storm track plays a role in the poleward extension of the summertime subtropical high (Miyasaka and Nakamura 2010).

The Subantarctic front (ACC-SAF) is the most equatorward feature of the ACC, which is continuous across the major oceanic basins (Fig. 1; Table 2) and about 30,000 km long (Rintoul and Naveira Garabato 2013; Orsi et al. 1995). The location of the ACC-SAF ranges from roughly equal (41°S) to much higher latitudes (60°S) than that (40–45°N) of the SAFZ in the Northern Hemisphere, and the SST and its gradient are partly similar to those of the SAFZ. The baroclinic transport associated with the ACC-SAF is estimated to be 53 Sv through the Drake Passage (Cunningham et al. 2003) and 105 Sv south of Australia (Sokolov and Rintoul 2007), while the total transport at each section is 137 Sv and 147 Sv, respectively. Hence, the ACC-SAF transport is comparable or larger than the transport of K-SOJ. On its encounter with southward-flowing western boundary currents of subtropical gyres, the ACC system enhances the SST gradient around the Brazil-Malvinas confluence and ARC (Table 2). The presence of the high SST gradients is considered to be essential in anchoring the storm track and polar front jet of the overlying atmosphere (Nakamura et al. 2004; Nakamura and Shimpo 2004; Hotta and Nakamura 2011; Ogawa et al. 2012), as could be seen in the KE region. The air–sea coupling associated with the storm tracks in turn can contribute to the maintenance of the fronts in both the ACC and KE regions through the downward transfer of westerly momentum and driving the ACC and oceanic gyres (Nakamura et al. 2004).

4 Kuroshio–Oyashio confluence region

In the region north of the KE, eddies, filaments, and jets, separated or bifurcated from the main streams of the Kuroshio and the Oyashio, merge and re-diverge frequently. We will refer to the region where waters that originate from each current mix, from the SAC to the KE, as the KOC region (Fig. 2).[1] While there are various terminologies used to describe the region, we will make an effort to follow the nomenclature provided by Favorite et al. (1976). Footnotes are added where different names have been used to indicate the same hydrographic feature discussed in this section. Readers are referred to Yasuda (2003) for a detailed review of the hydrographic structure in this area.

Though hydrographic features in this region are complicated, there are several distinct fronts and jets (Figs. 4, 6; Table 3). The broad region of large meridional gradients of SST [about 1.5 °C (100 km)$^{-1}$ around 40°N (WOA09), see also Fig. 4b; Table 3] and SSS [about 0.2 (100 km)$^{-1}$, see Yuan and Talley 1996) in the northern part of the KOC region is called the SAFZ.[2] In synoptic sections, the northern (southern) boundary of the SAFZ is marked by the outcrop of the 33.0 (33.8) isohaline, which forms the top (bottom) of the subarctic permanent halocline (Yuan and Talley 1996; see also Fig. 6). The SAFZ corresponds to the boundary between the wind-driven gyres of the North Pacific (e.g., Hurlburt et al. 1996). The SAFZ contains a couple of sharp SST and SSS fronts (Fig. 4b) with the SST and SSS gradients compensating each other in terms of density change. The SST gradient in the SAFZ is shown to have appreciable influence on the large-scale atmospheric circulation extending into the upper troposphere in the time mean (Nakamura et al. 2004; Taguchi et al. 2009) as well as time-varying states (Frankignoul et al. 2011; Taguchi et al. 2012; Smirnov et al. 2015). The near-surface baroclinicity maintained by differential heat exchanges across the oceanic front anchors the storm track (Nakamura et al. 2008; Sampe et al. 2010; Hotta and Nakamura 2011), and its modulation associated with latitudinal shifts of the oceanic fronts exerts eddy feedback forcing on the mean atmospheric circulation (e.g., Nakamura et al. 2004, 2008; Taguchi et al. 2009, 2012; O'Reilly and Czaja 2014).

The SAC or extension of the Oyashio and the northern branch of the KE or KENB[3] are well known as the persistent jets in the KOC region. The SSH gradient suggests frequent bifurcation and confluence of jets (Fig. 4a). Nevertheless, the pathways of these two currents may be traced from the east coast of Japan as far east as 170°E by using subsurface temperature proxies. In the northern part of the KOC region, the 4 °C isotherm at 100 m depth (Favorite et al. 1976) traces the southern boundary of the SAC well in the western and central portions of the North Pacific. This isotherm is the formal proxy of the southern limit of the "pure" subarctic stratification with a subsurface temperature minimum underlain by a temperature maximum (Belkin et al. 2002), which is termed as the Subarctic Front (SAF) by Ueno and Yasuda (2000) and Yasuda (2003).[4] Further, recent studies based on satellite observations have identified two remarkable quasi-stationary jets in the SAFZ immediately south of the SAC [Isoguchi et al. 2006; J1 and J2 in Figs. 4a and 6; see also Wagawa et al. (2014) for a recent hydrographic observation]. Across these quasi-stationary jets (Fig. 4b) the SST gradients exceed 4–5 °C (100 km)$^{-1}$, which marks the strongest gradients within the SAFZ and tends to be stronger than that associated with the KE (Nonaka et al. 2006).

In the southern part of the KOC region, the KENB originates from the KE, which can be identified by the 6–8 °C isotherms at 300 m depth (Mizuno and White 1983). From around 160°E, the KENB merges with another large SSH gradient, which extends eastward from about 150°E, 39°N (Fig. 4a). The latter roughly coincides with the subarctic boundary,[5] which is defined by the near vertical 34.0 isohaline in the surface layer within 38°–40°N (Favorite et al. 1976). Zhang and Hanawa (1993) showed that the KENB broadly corresponds to the subarctic boundary east of 170°E. Note that the subarctic boundary approximates the southern boundary of the SAFZ (Fig. 6b). Salinity increases with depth north of the subarctic boundary as in the subarctic North Pacific. The area between SAC and the subarctic boundary, which is called the Transition Domain (Favorite et al. 1976), has unique water properties much warmer and saltier than subarctic water.

Within the SAFZ, the SST fronts are observed throughout the year even in summer (Fig. 4c, d; see also Nakamura and Yamagata 1999). They become most prominent in winter and early spring. In winter, turbulent latent and sensible heat fluxes are locally maximized on the southern

[1] This name is also used by Sugimoto and Hanawa (2011), but many other names have been used to indicate this region, for example, the Perturbed Area (e.g., Kawai 1972), the Mixed Water Region (e.g., Talley et al. 1995), the Kuroshio-Oyashio interfrontal zone (e.g., Yasuda et al. 1996), and the Kuroshio-Oyashio Extension region (e.g., Schneider et al. 2002), etc.

[2] The SAFZ almost coincides with the region conventionally termed the Transition Domain in the oceanographic community (Favorite et al. 1976), which is bounded by the SAC and the subarctic boundary, which are described later in this section (see also Fig. 6).

[3] The northern branch of the KE (Mizuno and White 1983) is also called the Kuroshio Bifurcation front (Yasuda 2003) or the Kuroshio northern branch (Hurlburt and Metzger 1998).

[4] Roden et al. (1982) and Belkin et al. (2002) termed this front "the Polar Front."

[5] Roden et al. (1982) termed this boundary "the Subarctic Front."

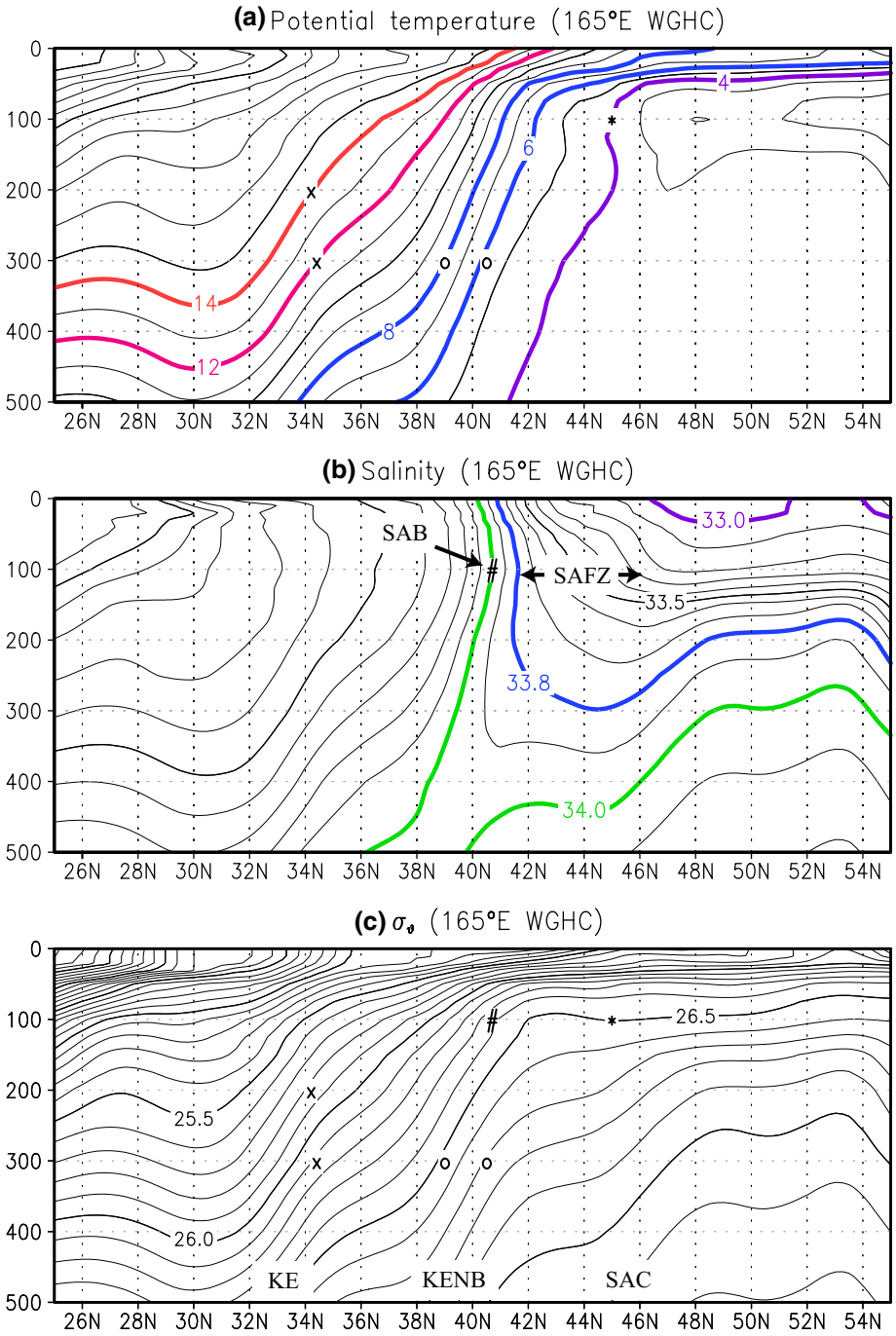

Fig. 6 Latitude-depth sections along 165°E of **a** potential temperature (°C), **b** salinity, and **c** potential density σ_θ (kg m^{-3}) based on WOCE Global Hydrographic Climatology (Gouretski and Koltermann 2004). Proxies for the locations of fronts used in Fig. 4b are also indicated by *marks*. The *crosses* mark the position of KE defined by the 14 °C isotherm at 200 m depth and the 12 °C isotherm at 300 m depth. The *circles* mark the position of KENB defined by the 6 and 8 °C isotherms at 300 m depth. The *sharp* marks the position of the subarctic boundary defined by the salinity of 34.0 at 100 m depth. The *asterisk* marks the position of the SAC defined by the 4 °C isotherm. The outcrop of isohaline of 33.8 (33.0) in **b** defines the southern (northern) boundary of SAFZ

flank of the quasi-stationary jets (Tomita et al. 2011; see also Fig. 4e, f), sharply declining northward across the jets (J1 and J2 in Fig. 4a). The surface baroclinic jets can be identified throughout the year, but positions of SAC and KENB vary significantly on short time scales owing to the effect of mesoscale eddies. In relation to the huge amount of wintertime heat release into the atmosphere in the vicinities of these fronts (Fig. 4e, f), several kinds of pycnostad, or mode water, are identified in the KOC region. Readers are referred to Oka and Qiu (2012) for a review. Reproducibility of mode waters in this region is a good metric for evaluating the fidelity of model simulations. Mode waters in model simulations may be evaluated by comparing the distribution of the isopycnic potential vorticity (PV) (Fig. 5 of Suga et al. 2004), subduction rate (Fig. 5 of Suga et al. 2008), and θ–S relationship for the deep winter mixed layer in the mode water formation region (Fig. 2 of Oka et al. 2011) with observations.

On interannual to decadal time scales, the latitudinal positions of SAC and KENB vary by about ±2° (Belkin

et al. 2002; Nakamura and Kazmin 2003; Nonaka et al. 2006). The dual jets identified by Isoguchi et al. (2006) are quasi-stationary in their flow directions, but the western jet (J1) varies on decadal scale synchronously with the meridional migration of KE (Wagawa et al. 2014). Isoguchi et al. (2006) suggested a possibility of bottom topography effects on the steady direction of the current, although no obvious interaction of the jet with the bottom topography was found in a snapshot observation (Wagawa et al. 2014).

The westernmost portion of the front that traces the southern boundary of the SAC is specifically called the Oyashio front, which marks the southern edge of the western subarctic water where subsurface salinity is <33.6. Kawai (1972) thus suggested the 33.7 isohaline at 100 m depth as an index of the Oyashio front. In terms of temperature, Kawai (1972) suggests a 7 °C isotherm in January, 6 °C in February, 5 °C from March to May, 6 °C from June to August, 7 °C from September to October, and 8 °C from November to December at 100 m depth. As discussed by Yasuda (2003), the Oyashio front is known to have two branches intruding southward adjacent to the east coast of Japan, exhibiting large seasonal and interannual variations. We will not pursue metrics for the Oyashio front beyond these indices owing to its overwhelmingly complex behavior.

5 Fronts in the subtropical North Pacific

5.1 Northern, Southern, and Eastern subtropical fronts

An STF is a subsurface temperature and density front at depths of about 50–300 m, accompanying a steep northward shoaling of the upper pycnocline (Fig. 7a). The slope of the upper pycnocline gives rise to the eastward current shear of the Subtropical Countercurrent (STCC) near the surface in opposition to the barotropic westward flow predicted by the Sverdrup theory at these locations. The STCC is a shallow current and is usually found above the core depth of the STF (Fig. 7b).

There are three STFs in the North Pacific (Fig. 2), and they are basically maintained by different mode waters in the ventilated thermocline (Kubokawa 1999; Aoki et al. 2002; Kobashi et al. 2006; Kobashi and Kubokawa 2012). The STCCs associated with the Northern and Southern STFs show a distinct seasonal cycle in velocity with a maximum in spring and minimum in autumn, whereas the STCC associated with the Eastern STF exhibits no significant seasonal cycle (Table 4). Each of the STFs forms a vertically sheared current system between the STCCs and an underlying westward flow, which favors high eddy activity. The EKE undergoes significant seasonal modulation with a maximum in May and minimum in December through January, reflecting the seasonal change in the dynamical stability of the sheared current system (Qiu 1999; Kobashi and Kawamura 2002), which is modified by the presence of the SST front in the mixed layer (Chang and Oey 2014). The EKE also changes considerably on interannual and decadal timescales (Qiu and Chen 2010b, 2013) because of the large variability of the STCCs (Table 4).

In some literature, STFs refer to SST fronts (e.g., Roden 1980). Different from the subsurface STFs, SST fronts are relatively broad and form in response to surface Ekman convergence and/or inhomogeneity in surface heat fluxes (Kazmin and Rienecker 1996; Dinniman and Rienecker 1999; Qiu and Kawamura 2012). Satellite data reveal a local peak of the SST gradient embedded in a broad surface frontal zone along the Northern and Eastern STFs. The surface front exhibits the strongest SST gradient in February through March and the weakest in August through September. Probably anchored by the subsurface STFs, the SST front enhances the overlying atmospheric baroclinicity and thereby influences surface wind stress curl and precipitation (Kobashi et al. 2008). The Northern and Eastern STFs also accompany a weak but notable local peak of upward sensible heat flux in spring along the northern front and in winter and spring along the eastern front (Fig. 8). Some coupled general circulation model (GCM) studies indicate that the thermal advection of STCCs may yield SST anomalies leaving imprints on surface heat flux and surface winds (Xie et al. 2011).

Salinity is considered to make a minor contribution to STFs because of relatively warm water in the subtropics. At the surface, the Northern and Eastern STFs are roughly located along the maximum of high-salinity Tropical Water, whereas the Southern STF is along the southern flank of Tropical Water. The salinity gradient does not exhibit significant seasonal changes at the surface (Table 4). At subsurface depths, the Northern and Eastern STFs are observed along the northern boundary of Tropical Water (Uda and Hasunuma 1969; Kobashi and Kubokawa 2012), where the salinity front could weaken the density front, because temperature and salinity have opposing effects on density.

5.2 Hawaiian Lee Countercurrent

The HLCC (Flament et al. 1998) is a narrow surface eastward current, extending far westward from Hawaii against the easterly trade winds and broad westward North Equatorial Current (Fig. 2). The western end of the current has significant interannual variations. Climatologically, it is found around 170°W–175°W from drifting buoy observations (Qiu et al. 1997; Yu et al. 2003; Lumpkin and Flament 2013; Abe et al. 2013) and a bit further westward over the international dateline to about 165°E from

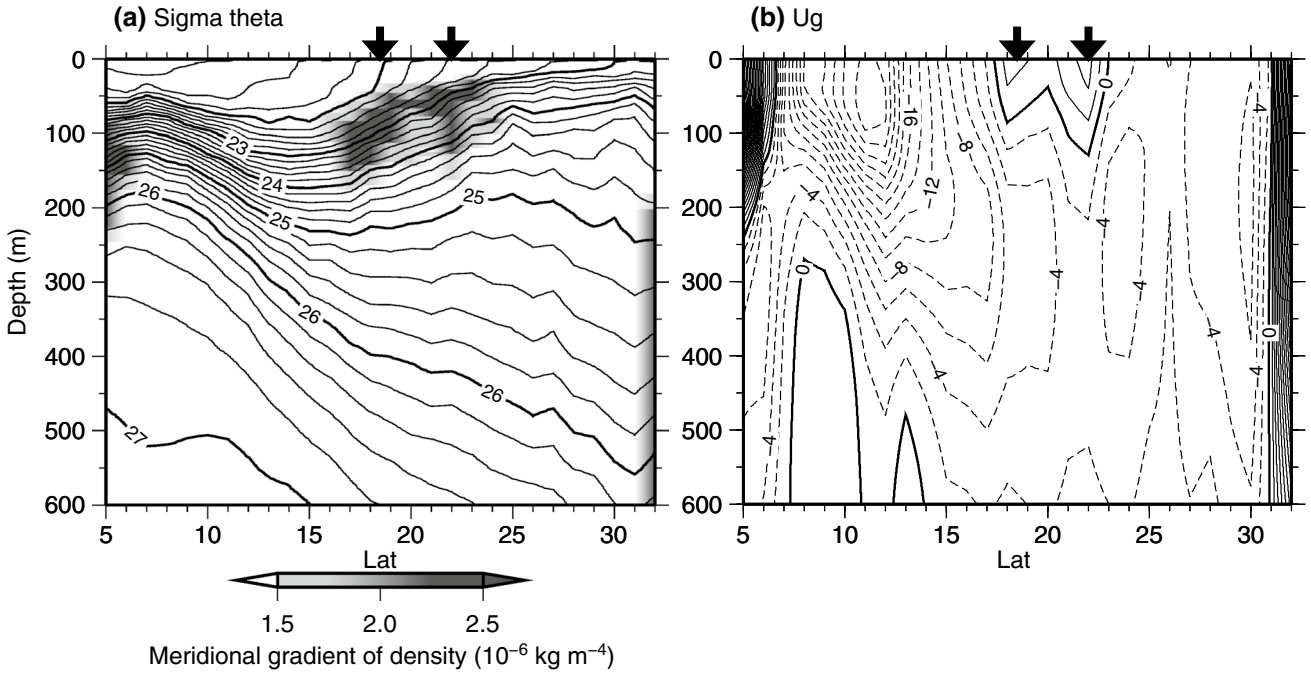

Fig. 7 Mean sections of **a** potential density and **b** zonal geostrophic velocity (referenced to 1000 dbar) along 137°E, calculated from CTD observations every winter and summer season during 2000–2009, conducted by the Japan Meteorological Agency. *Shade* indicates the meridional gradient of potential density. Stations along the sections are located approximately 1° apart in latitude. The locations of the Northern and Southern STFs (STCCs) are denoted by *arrows*. Modified from Kobashi and Kubokawa (2012)

altimeter observations (Sasaki et al. 2010; Abe et al. 2013) and hydrographic observations (Kobashi et al. 2006). The current is accompanied by subsurface temperature and density fronts, but the SST along the current is warm compared to that of surrounding water because of the warm water advection from the west (Fig. 8b).

Although the HLCC flows at almost the same latitudes as the STCC, which is associated with the Southern STF (Fig. 2), the generation mechanism is quite different. The HLCC is a basically wind-driven flow and is generated by the wind wake near Hawaii (Xie et al. 2001). The Rossby waves, triggered by the dipole pattern of the surface wind curl near Hawaii, propagate westward to induce the front with surface eastward current. The extent of more than a few thousand kilometers is the longest among the currents (with fronts) triggered by the orographic wake on earth. The speed of the HLCC varies seasonally, remaining strong from summer through winter and weakened in spring (Kobashi and Kawamura 2002), induced by meridional migration of the trade winds (Sasaki et al. 2010). Interannual variations of the current are attributable to variations of the northward extent of low-PV water (Sasaki et al. 2012b) and/or to westward Rossby wave propagations from the east of Hawaii triggered by wind anomalies (Abe et al. 2013). However, further studies are needed to reveal the dominant mechanism of the variations.

The SST maximum associated with the HLCC creates upward sensible and latent heat fluxes (Table 4; Fig. 8b) and induces surface wind convergence and high cloud water over the HLCC (Xie et al. 2001). The magnitude of the heat fluxes is comparable to that along the STFs (Table 4). The wind convergence, together with the Coriolis force, enhances (weakens) the easterly trade winds to the north (south), which may shift the SST maximum southward via the thermal feedback of latent heat release (Xie et al. 2001). A comparison of coupled GCM experiments with and without the SST maximum further suggests that the HLCC is accelerated, extended further westward, and shifted southward by the dynamical feedback of Ekman suction that is associated with the positive wind stress curl along the HLCC via the thermal wind balance (Sasaki et al. 2013). Such dynamical feedback associated with the increase of HLCC can potentially intensify the seasonal and interannual variations.

The HLCC, as well as STCCs, forms a vertically sheared current system with underlying westward flow. Reflecting seasonal variations of the baroclinicity of the sheared current, the EKE tends to be high from spring to early summer and low in winter (Kobashi and Kawamura 2002; Yoshida et al. 2011). The EKE also varies on interannual and decadal time scales. A high EKE was observed

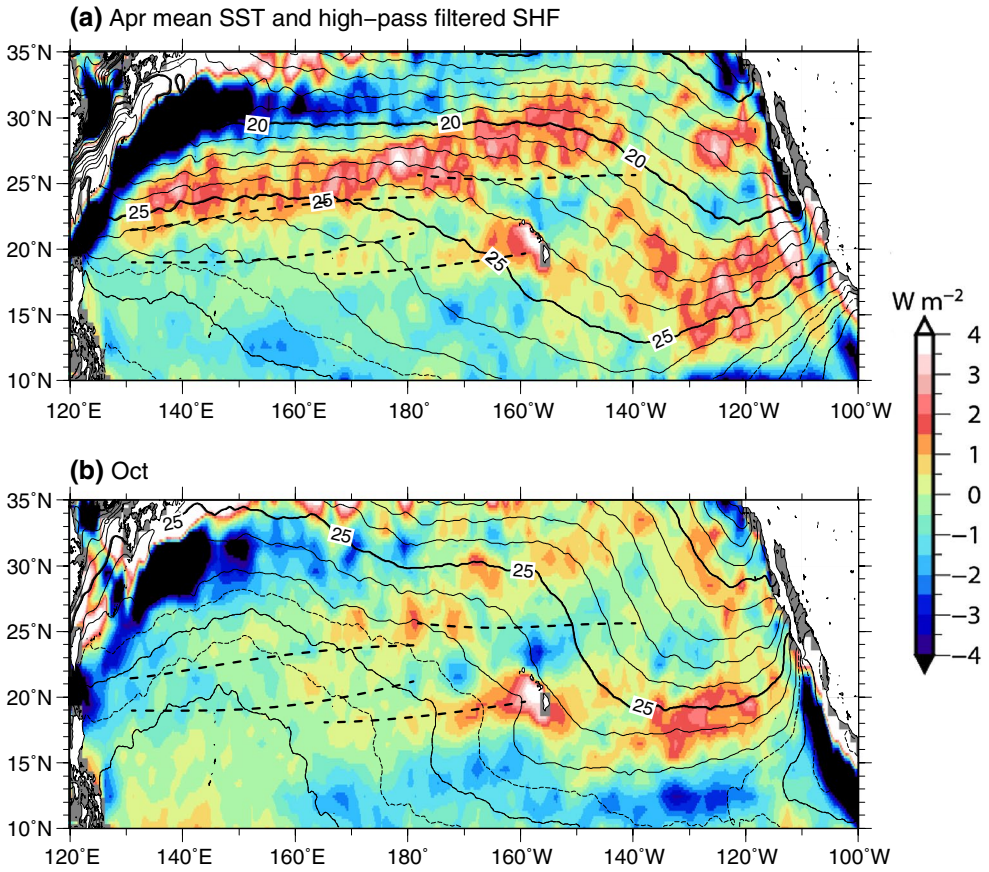

Fig. 8 Mean SST (*contours*) as well as high-pass filtered sensible heat flux (*color*; W m^{-2}) in **a** April and **b** October. SST is contoured every 1 °C with thin *dashed contours* of 0.5 °C intervals over 27 °C. The high pass filtering is done by subtracting a 10° moving average in latitude from the original data to remove the large-scale background distribution. *Thick dashed lines* indicate the climatological location of the STFs and HLCC

in 1993–1998 and 2002–2006, while the EKE was low in 1999–2001 and 2007–2009. During the positive PDO phase, cold SST anomalies north of the current, induced by enhanced heat loss to the atmosphere, augment the vertical shear and thereby enhances the EKE (Yoshida et al. 2011).

6 Fronts in coastal and marginal seas

6.1 Tidal fronts of the Seto Inland Sea

There are two types of thermal fronts in the Seto Inland Sea. One is a tidal front in summer, and the other is a thermohaline front in winter (Yanagi and Koike 1987). As reflected in its name, a tidal front is associated with tidal currents. It is produced by surface warming in coastal seas, where spatial variations in tidal currents are strong. Water is vertically mixed where tidal currents are strong, whereas water is stratified where tidal currents are weak. Between these two regions, a tidal front thus forms with a pronounced water temperature gradient (Simpson and Hunter 1974).

A number of tidal fronts are observed in the Seto Inland Sea (Takeoka 2002). As a typical example, a front around Hayasui Strait (Yanagi and Koike 1987) is included in Table 5 (see also the inset panel of Fig. 2). The particular front can be identified from late April to early September. The front has a length of about 40 km and width of about 5 km across which the SST changes by 2 °C and the SSS by 0.3. The SST gradient undergoes a fortnightly variation: being stronger in the spring tide than in the neap tide (Yanagi and Koike 1987), whose dynamical explanation is given in Sun and Isobe (2006).

Among thermal fronts with different spatial scales (Yanagi 1987), tidal fronts are one of the smallest types of oceanic fronts that can influence the overlying PBL structure (Shi et al. 2011). The surface wind speed reduces when the air travels from the warm to cooler water and vice versa, which is mainly because of the perturbation pressure gradient force with the SST gradient and not the stratification control on the turbulent vertical mixing of wind momentum (Shi et al. 2011).

6.2 Japan Sea subpolar front

The JS-SPF (Fig. 2; Table 5) is the boundary between the warm and salty water mass entering from the Tsushima Strait and the cold and fresh water mass formed within the Japan Sea (Isoda et al. 1991; Talley et al. 2006). This front is sometimes referred to as the polar front (e.g.,

Isoda 1994), and the presence of the JS-SPF has long been recognized (Uda 1938), owing possibly to its prominent frontal signal extending zonally across the Japan Sea at 40°N throughout the year. Satellite observations show bifurcations at its eastern and western ends, which are near the coasts and where variability is stronger than in the interior (Park et al. 2004). Due to the depth of the Japan Sea, the JS-SPF shares many common features with its counterpart in the open ocean. For example, the front is considered a region of intense subduction and thus intermediate water formation. This has led to intense studies on the mechanism of frontal subduction during the last decade or so (Thomas and Lee 2005; Yoshikawa et al. 2001; Lee et al. 2006).

Although relaxed substantially in summer, the SST gradient across the subpolar front is strong particularly in winter, locally observed to reach as high as 5 °C over 5 km at times (Lee et al. 2006), with climatological values comparable to or even stronger than that across the KE (Table 1). Likewise, upward turbulent heat fluxes at the surface are strong in winter, especially to the south of the subpolar front (Fig. 4e, f), where direct observations show the heat fluxes frequently exceeding 300 W m^{-2} (Lee et al. 2006). Adjacent to the Asian continent, the large amount of heat loss from the Japan Sea occurs under the monsoonal cold air outbreaks. In addition to this strong surface cooling of the warm water, strong cold Ekman advection across the sharp SST gradient results in the destabilization of the near-surface stratification in the ocean and contributes to the frontal genesis (Thomas and Lee 2005; Lee et al. 2006). As the response of the atmospheric PBL to the frontal SST gradient and associated cross-frontal differential heat release, the surface wind speed is observed to be stronger over the warmer water, contributing to intense air–sea coupling in the region (Shimada and Kawamura 2006, 2008). Furthermore, Shimada and Kawamura (2006) showed an atmospheric response to the SST front induced by the Tsushima Current located to the south of the JS-SPF.

The JS-SPF is also associated with an eastward jet observed to be about 0.30 m s^{-1} at the surface (Isobe and Isoda 1997). Observational analysis shows an annual mean transport of about 1.1–1.2 Sv (Chu et al. 2001), which is embedded in the general northeastward flow of the Tsushima Current. The JS-SPF corresponds to the boundary between this eastward flow to its south and the cyclonic gyre to its north. Climatological EKE does not exhibit a maximum along this front but rather an increasing tendency toward its south (Jacobs et al. 1999). The JS-SPF is observed to vary interannually and decadally, which is possibly induced by instability of the jet, the anomalous in/outflows through the straits, and basin-scale atmospheric variability (e.g., Isoda 1994; Minobe et al. 2004). Recent studies suggest that the SST variability in the Japan Sea may, in return, affect large-scale atmospheric circulation (Yamamoto and Hirose 2011), although fine-structure SST anomalies may not be quite relevant in forcing large-scale atmospheric anomalies (Seo et al. 2014b).

7 Summary and concluding remarks

This article reviewed the progress in our understanding of oceanic fronts around Japan that has accumulated in the recent years and summarized the frontal properties in Tables 1, 2, 3, 4, and 5. In addition to simply serving as a reference list of the metrics, Tables 1, 2, 3, 4, and 5 can be used for visualizing the characteristics of fronts. For example, a scatter plot of the metrics using the SST gradient and flow speed shows how the frontal structure may compare with other fronts (Fig. 9a). From the thermal wind balance, the surface flow speed should be stronger as the density gradient increases or thickness of the front increases, assuming the flow is weaker at depth. Therefore, if density is primarily a function of temperature, the upper part of the plot shows the fronts where thickness is likely playing a large role, such as the major western boundary currents. Fronts such as the JS-SPF show a strong SST gradient but weak flow speed likely because of their shallow structure. Note, however, that salinity likely plays a large role for the fronts in the KOC region and that latitudinal differences need to be considered for more detailed analysis. A similar scatter plot can be created using the metrics for the SST gradient and sensible heat flux (Fig. 9b). Enhanced heat fluxes are expected in the vicinity of an ocean front when air parcels travel across the front, since their temperature requires additional time to adjust to the underlying SST (see also Fig. 15 of Small et al. 2008). The stronger the SST gradients become, the larger the difference between the SST and surface atmospheric temperature (SAT) become, which then results in enhanced sensible heat flux. The scatter plot appears to suggest such a trend, although there are also significant differences among the fronts. The difference between the SST and SAT may well be present on the large scale due to factors such as large-scale wind speed and the distance from land, likely making the actual magnitude of the heat fluxes differ depending on the front.

One of the metrics that is missing from Tables 1, 2, 3, 4, and 5 is the frontal variability on time scales longer than the interannual scales. The KE, for instance, is known to exhibit pronounced decadal-scale variability in frontal location and intensity. How much the metrics differ between the varying states would be an interesting aspect

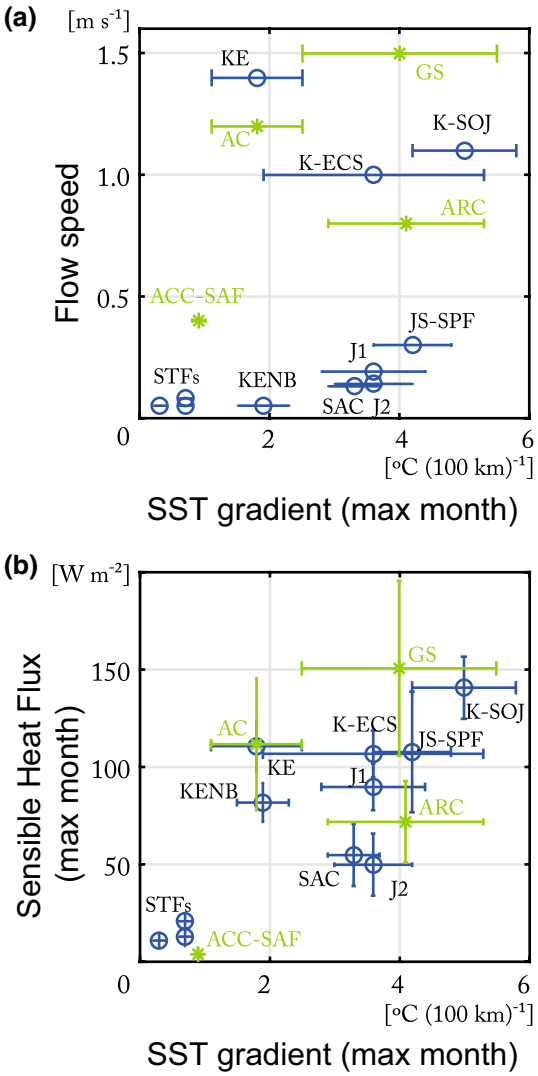

Fig. 9 **a** Scatter plot of the SST gradient (maximum month) and flow speed based on Tables 1, 2, 3, 4, and 5. The *bars* indicate the magnitude of interannual variability. *Blues* are the fronts in the North Pacific. *Greens* are the fronts located elsewhere. **b** Same as **a** except for the SST gradient (maximum month) and sensible heat flux (maximum month)

to compare in the future. While we hope the metric table will be useful, two aspects need to be kept in mind. First, redefinition of the metrics may be necessary when evaluating numerical models because model outputs often contain biases. For example, an eddy-resolving ocean GCM (OFES; Masumoto et al. 2004; Sasaki et al. 2008) successfully reproduces the KE and KOC region including three-separated surface and subsurface temperature and/or SSH fronts (e.g., Nonaka et al. 2006). However, the location of the KE and KENB was better defined by the location at 300 m depth of the 14 and 10 °C isotherms rather than 12 and 8 °C (see Sects. 3.1.1 and 4 for the metrics of KE and KENB), respectively, since the model had subsurface warm bias in this region. Second, we need to be cautious not to oversimplify the metrics, although they are useful. Some of the conventional metrics are also based on temperature because of its data availability and that they may have been originally defined by other variables. For example, Kawai (1972) proposed the metric for describing the location of the Oyashio front by the 33.7 isohaline at 100 m depth. To interpolate this isohaline from the temperature field, different isotherms needed to be chosen for each calendar month. In some literature, however, the definition has been oversimplified by the use of the 5 °C isotherm at 100 m depth throughout the year. This is clearly no longer the same as the original definition proposed by Kawai (1972).

Oceanic fronts are now reasonably well resolved in recent high-resolution ocean GCMs and just beginning to be resolved by high-resolution global air-sea coupled models. We envision that some of the coupled GCMs contributing to the next Assessment Report of the Intergovernmental Panel on Climate Change (IPCC) will represent oceanic fronts reasonably well. We need to assess what significant impacts can be exerted in the mean state and variability of the model-simulated atmospheric and oceanic circulation by the improved representation of oceanic fronts. We hope that the metric tables (Tables 1, 2, 3, 4, and 5) can provide a useful tool for evaluating the fronts captured in the state-of-the-art numerical models.

Acknowledgments We thank the editor, Dr. Shoshiro Minobe, and three anonymous reviewers for their constructive comments on the manuscript. The altimeter products are produced by Ssalto/Duacs and distributed by AVISO with support from CNES (http://www.aviso.oceanobs.com/duacs/). APDRC at the University of Hawaii at Manoa (http://apdrc.soest.hawaii.edu/) was also used to obtain some of the data sets. This work is supported by the Japan Society for Promotion of Science through a Grant-in-Aid for Scientific Research on Innovative Areas 2205.

Appendix

The methods and data sets used for estimating the metrics shown in Tables 1, 2, 3, 4, and 5 are described here. Common data sets used for the SST and its gradient are monthly means of AMSR-E SST (Gentemann et al. 2010), MGDSST (Kurihara et al. 2000), and OISST (Reynolds et al. 2007) from 2003 to 2008. Monthly climatology of WOA05 (Antonov et al. 2006), WOA09 (Antonov et al. 2010), and WOA13 (Zweng et al. 2013) is used for the SSS and its gradient. Monthly means of AVISO (http://www.aviso.oceanobs.com/duacs/) from 1993 to 2007 are used for the SSH gradient and EKE. The J-OFURO2 (Tomita et al. 2010) from 1993 to 2007 is used for the surface heat fluxes. Specific data sets used for each front are shown in Table 6, and detailed differences are described

Table 6 Data sets and references used for estimating the metrics associated with the SST, SSS, and their gradients, SSH gradient, and heat fluxes in Tables 1, 2, 3, 4, and 5

	Kuroshio			GS	AC and ARC	ACC-SAF	KENB, SAC, J1, J2, and SAFZ
	KE	K-SOJ	K-ECS				
SST, ΔSST	MGDSST	MGDSST	PN line (JMA)	AMSR-E SST	AMSR-E SST	Reynolds SST	AMSR-E SST
SSS, ΔSSS	WOA13	WOA09	PN line (JMA)	WOA09	WOA05	WOA09	WOA13
ΔSSH	AVISO	AVISO	AVISO	AVISO	AVISO	Sallee et al. (2008)	AVISO
Heat flux	J-OFURO2	J-OFURO2	J-OFURO2	J-OFURO2	J-OFURO2	J-OFURO2	J-OFURO2

	NSTF, SSTF, and ESTF	HLCC	Seto Inland Sea tidal front	JS-SPF
SST, ΔSST	Reynolds SST	Reynolds SST	Yanagi and Koike (1987)	AMSR-E SST
SSS, ΔSSS	WOA09	WOA05	Yanagi and Koike (1987)	WOA13
ΔSSH	AVISO	AVISO	Takeoka (2002)	AVISO
Heat flux	J-OFURO2	J-OFURO2	Chang et al. (2009)	J-OFURO2

below. Other metrics are primarily based on past observational studies.

Kuroshio Extension

The location of the KE is based on the regions defined in Qiu and Chen (2005). Since the behavior of the frontal axis is significantly different between the upstream and downstream, two metrics are provided. One is the average over the whole frontal axis and the other is that limited to the upstream. The frontal axis is determined from the maximum flow speed based on the methods described in Ambe et al. (2004). FRA-JCOPE2 utilizes the flow speed at 10 m depth. SST and its gradient are estimated from MGDSST (1993–2007). SST is estimated by averaging the SST 50 km north and south of the frontal axis, and the SST gradient is estimated by taking the difference between the two. However, we exclude the months when the KE axis is obviously obscured by the presence of a meso-scale eddy or the method detects the KENB instead. SSS and its gradient are estimated from WOA13 using similar methods as the SST and its gradient, respectively. However, only the upstream values are presented since WOA13 is a climatology and thus unable to capture the transient variability of the frontal axis downstream. Only the upstream values, where variability is less, are presented. The SSH gradient is estimated from the monthly means of AVISO, but the annual mean is presented since the magnitude of the SSH gradient does not change significantly with seasons. Other dynamical properties are based on observational studies. Transport and flow speed are both based on Howe et al. (2009), which are observations from 146°E. Note that the transport decreases significantly to about 75 Sv at 148.5°E. Depth is determined from WOCE hydrography (http://www-pord.ucsd.edu/whp_atlas/pacific_index.html). The EKE is based on the downstream and upstream values estimated from satellite altimetry in Qiu and Chen (2005). Heat fluxes are estimated from the J-OFURO2 by taking a spatial average between 141°–163°E and 34°–38°N to represent the whole KE region and 141°–153°E and 34°–38°N to represent the upstream KE region.

Kuroshio south of Japan

The location of the Kuroshio axis is estimated from the monthly mean SSH derived from AVISO. Using the SSH gradient, the latitudinal position of the Kuroshio axis is determined at each longitude with an interval of 0.25° between 131° and 140°E. The SSH gradient is then calculated by taking a zonal average of the gradient at this Kuroshio axis. SST and its gradient are estimated from monthly means of MGDSST using a similar method. Since the SST front associated with the Kuroshio is not closely matched with the current axis as mentioned in Sect. 3.2, the position of the SST front is determined from the maximum SST gradient within the region between 1° south and north of the current axis defined from the SSH. The SSS and its gradient are estimated from monthly climatology of WOA09 and are determined as the maxima around the mean Kuroshio axis. The length of the K-SOJ is estimated between 131° and 140°E using the Kuroshio axis data set of Ambe et al. (2004) from 1993 to 2007, which includes periods of both straight and large meander paths. Flow speed and transport are from observations by Ambe et al. (2004) and Imawaki et al. (2001), respectively. While the estimates of the Kuroshio transport tend to be contaminated by local phenomena such as the Kuroshio path variations and mesoscale eddies, the transport value presented in Imawaki et al. (2001) was observed off-shore of Shikoku where the Kuroshio is relatively stable. The depth of the Kuroshio is based on observations by Book et al. (2002). The EKE is estimated from the monthly mean geostrophic velocity anomaly of AVISO.

Heat fluxes are estimated from the J-OFURO2 by taking a spatial average within 131°–140°E and 30°–35°N. The dynamical properties, such as the SSH gradient, flow speed, transport, and EKE, do not change significantly with seasons and thus are presented by their annual means.

Kuroshio along the shelf break of the East China Sea

The location of the K-ECS follows the current field given by Qiu et al. (1990) with the exclusion of the Kuroshio northeast of Taiwan because there is no apparent thermal front there (HicKox et al. 2000). SST, SSS, and their gradients are based on quarterly hydrographic data along the PN line in January, April, July, and October from the period of 1980–2012, provided by the Japan Meteorological Agency (http://www.data.jma.go.jp/kaiyou/db/vessel_obs/data-report/html/ship/ship.php). The SSH gradient is estimated from the monthly means of AVISO with the Kuroshio axis defined by the location of the maximum SSH gradient between 124° and 127°E. Heat fluxes are also estimated along this Kuroshio axis from the monthly means of the J-OFURO2. Flow speed, transport, and depth are based on observations by Oka and Kawabe (1998). The EKE is based on numerical simulations by Miyazawa et al. (2004).

Gulf Stream

All values are based on the GS after the separation at Cape Hatteras, where the location of the GS frontal axis is based on Sasaki and Schneider (2011): The jet latitude is defined as a contour of −10 cm from absolute dynamic topography data by Niiler et al. (2003b). SST and its gradient are estimated from the monthly means of AMSR-E SST, where the gradient is based on values 2° north of the frontal axis averaged from 60°W to 70°W, and only the maximum month is presented. SSS and its gradient are estimated from the annual mean WOA09 averaged along the frontal axis and along 2° north of the frontal axis, respectively, from 60°W to 70°W. The SSH gradient and EKE are estimated from AVISO and are also annual means. The SSH gradient is at 70°W, and the EKE is estimated averaged along the frontal axis from 60°W to 70°W. The transport is based on the maximum value from in situ observations near 55°W by Hogg (1992). The depth is based on observations by Johns et al. (1995). Heat fluxes are estimated from the J-OFURO2 averaged along the frontal axis from 60°W to 70°W.

Agulhas Current and Agulhas Return Current

The location of the AC and ARC is based on Gordon (1985) and Lutjeharms and Ansorge (2001), respectively. Metrics related to SST, SSS, and SSH are estimated from AMSR-E SST, WOA05, and AVISO, respectively. SST and SSS are those found along the frontal axis and are estimated from the monthly means for SST, but the annual mean for SSS. The SST, SSS, and SSH gradients are maxima found along the frontal axis in the annual means. Heat fluxes are estimated from the J-OFURO2 along the frontal axis for the AC but maximum values within 15°E–60°E and 45°S–30°S for the ARC. Flow speed, transport, and depth are all based on observational studies by Bryden et al. (2005) for the AC and Lutjeharms and Ansorge (2001) for the ARC. The EKE is estimated from the monthly mean geostrophic velocity anomaly of AVISO.

Antarctic Circumpolar Current-Subantarctic front (ACC-SAF)

The location of the front is based on Orsi et al. (1995). SST and its gradients are estimated from the monthly mean OISST data from 1982 to 2011, with a spatial resolution of 1° by 1° (Reynolds et al. 2002). SSS and its gradient are estimated from WOA09 and are annual means. These estimates are the circumpolar averages along the fixed frontal location of Orsi et al. (1995). The dynamical properties are based on observational studies; the SSH gradient is from Sallee et al. (2008), flow speed is from Hofmann (1985), transport is from Rintoul and Sokolov (2001) and Cunningham et al. (2003), depth is from Tomczak and Godfrey (2003), and EKE is from Patterson (1985). Heat fluxes are estimated from the J-OFURO2 and are the circumpolar averages along the frontal axis.

Kuroshio-Oyashio confluence region

Metrics for KENB, SAC, J1, and J2 are estimated by averaging the respective parameters along the frontal axes associated with the location metrics in Table 3. The KENB axis is indexed by a straight line that connects its location metrics, which lies between 6 and 8 °C at a depth of 300 m, so as to be consistent with Mizuno and White (1983). The metrics are estimated within 153°–170°E, where the axis is distinctly separated from KE (Fig. 4a). The SAC axis is defined by 4 °C isotherms at 100 m depth (Favorite et al. 1976; Belkin et al. 2002). The metrics of SAC are estimated within 150°–155°E along the 4 °C isotherm as a typical value where the SST gradient is maximum [typically >3 °C (100 km)$^{-1}$ in winter], although the front extends farther eastward. J1 and J2 are indexed by straight lines that connect their location metrics; these lines are located immediately southward of the maximum SST gradients [typically >3 °C (100 km)$^{-1}$ in winter] in the SAFZ north of 40°N (Fig. 4c). The SST and its gradient for KENB, SAC, J1, and J2 are estimated from the monthly means of AMSR-E SST (Figs. 4c, 3d). SSS and its gradient for KENB, SAC, J1, and J2 are estimated from

the monthly climatology of WOA13. The SSH gradients and surface currents are estimated from the absolute SSH of AVISO (e.g., Rio et al. 2011). The EKE is based on the monthly mean surface geostrophic anomaly. Depths for KENB, J1, and J2 are based on Isoguchi et al. (2006). Transport for SAC is based on Ohtani (1970). Estimates of transport for other fronts are estimated from WOA13 based on geostrophy referenced to 1,500 m depth. Eastward flows that are parallel to the frontal axis are used. We are currently not aware of past studies to compare these values with, but the geostrophic velocity estimates near the surface match reasonably well with those of Isoguchi et al. (2006), as well as with those calculated from the AVISO SSH, and thus consider the transports reasonable to the first order. The difference between SAC and J1 is unclear in observational data sets where spatial smoothing is applied. Heat fluxes are estimated from the J-OFURO2.

For the metrics of SAFZ, SST is estimated along the line that connects (145°E, 40°N) and (180°, 45°N). SSS and its gradient are based on WOA13, and the heat fluxes are based on the J-OFURO2 along the same line. The SST gradient within the SAFZ is characterized by those of J1 and J2 and thus is not presented here.

Northern, Southern, and Eastern Subtropical fronts (NSTF, SSTF, and ESTF)

The locations of the STFs are determined from the AVISO reference series of the delayed-time Maps of Absolute Dynamic Topography (MADT) product from 1993 to 2007. STFs are defined as a continuous band of eastward surface geostrophic velocity in the monthly climatology. The climatology is still a bit patchy, probably because of high eddy activity, but the positions of the STFs show no clear seasonal variations. The eastern end of the SSTF is determined based on the climatology map of subsurface temperature fronts (Kobashi et al. 2006) because of the presence of the HLCC there. SST is estimated from the monthly means from an optimally interpolated SST data set produced from the blend of infrared and microwave satellite observations and in situ measurements from 2003 to 2008 (Reynolds et al. 2007). SSS is estimated from the monthly climatology of WOA09. SST, SSS, and their gradient are estimated at the current axis of the STCCs after calculating the zonal averages.

The flow speed is estimated from the surface eastward geostrophic velocity since the meridional velocity blurs the characteristic of the STFs. The meridional velocity is generally related to the basin-scale subtropical gyre circulation and has the same order as the zonal one at STFs. To estimate the metrics, zonal averages of zonal velocity are first calculated from the monthly mean each year between 145°E and 165°E for the N- and S-STFs and 175°W–155°W for the ESTF, and then the monthly climatology is estimated. We extracted a meridional peak of the velocity and its associated SSH gradient for each month. Since the ESTF shows no significant seasonal cycle, its metrics are estimated from the annual mean. The transport and depth are left blank because these metrics need information about the vertical extent of the fronts, which may not necessarily be easily accessible from observations. Synoptic ship observations (e.g., Aoki et al. 2002) appear to be inconsistent with altimeter-derived climatology when compared at the surface (see a review paper by Kobashi and Kubokawa 2012), probably because of observation sparsity and eddy contamination. The EKE is calculated from the monthly means of the geostrophic velocity anomaly. We first computed the monthly spatial averages of the EKE each year within 23°–25°N and 145°–165°E for the NSTF, 18°–20°N and 145°–165°E for the SSTF, and 25°–27°N and 175°–155°W for the ESTF, and then estimated the monthly climatology. Heat fluxes are assessed in the same way as the EKE using the monthly means of the J-OFURO2.

Hawaiian Lee Countercurrent

The location of the HLCC front is determined by examining the surface zonal geostrophic velocity relative to 400 db in climatological hydrographic observations (Kobashi et al. 2006). The western end changes interannually from the east of the international dateline to about 165°E from altimeter observations (Sasaki et al. 2010; Abe et al. 2013). When the HLCC and SSTF influence each other, the western extent of the HLCC cannot be determined clearly. SST is estimated from the monthly means of the OISST data set from 2003 to 2008 (Reynolds et al. 2007). The SST gradient is not provided since the SST shows a maximum along the HLCC. The SSS and its gradient are based on the monthly climatology of WOA05. The SSH gradient and surface flow speed are estimated from AVISO reference series of delayed-time MADT from 1993 to 2007 assuming geostrophy between 180 and 160°W at 19.5°N. The depth and transport are determined between 180° and 160°W with the transport estimated from the numerical simulations of the OFES Quikscat run (2001–2008) (Masumoto et al. 2004; Sasaki et al. 2008). The EKE is determined from Yoshida et al. (2011) between 170.0°E–160.0°W and 17.0°–21.7°N, which is based on AVISO SSH. Annual mean is presented with its variability estimated based on 1 year running weakly means. The seasonal EKE level peaks in June (0.025 $m^2\ s^{-2}$) and drops to a minimum in January (0.015 $m^2\ s^{-2}$). Heat fluxes are estimated from the monthly J-OFURO2 from 2002 to 2007.

Seto Inland Sea tidal front

The location, SST, SSS, and their gradients are based on observations during April by Yanagi and Koike (1987). The SSH gradient, flow speed, transport, depth, and EKE are based on the general knowledge of tidal fronts found in the Seto Inland Sea from observations and numerical models (e.g., Takeoka 2002; Chang et al. 2009). Heat fluxes are based on numerical simulations (Chang et al. 2009; Shi et al. 2011) for a limited period; thus, their interannual variability is not provided.

Japan Sea subpolar front

The location of the front is based on Park et al. (2004) where the JS-SPF does not include major bifurcations. The frontal axis is determined from the maximum SST gradient near 40°N from the monthly means of AMSR-E SST. SST and its gradient are the averages along this frontal axis. SSS and its gradient are estimated from the monthly climatology of WOA13 based on the monthly climatological position of the frontal axis. The SSS gradient is presented with a sign since the sign changes during the year. Positive values represent higher salinity toward the north. The SSH gradient is also estimated along the frontal axis using the monthly means of AVISO (2003–2008). Flow speed is based on direct observations by Isobe and Isoda (1997), and transport is based on inverse calculation using the observational data set by Chu et al. (2001). Depth is based on the observational analysis of Isoda (1994) and Minobe et al. (2004). The EKE does not show a clear maximum along the front (Jacobs et al. 1999) and thus is not presented. Larger values are found towards the south of the front, where the Tsushima Current exists, and the subpolar front appears to be much of a transition area from high (south) to low (north) EKE areas. Heat fluxes are estimated along the frontal axis using the monthly means of the J-OFURO2 (2003–2008).

FRA-JCOPE2

The Japanese Fishery Research Agency (FRA)-Japan Coastal Ocean Prediction Experiment (JCOPE) (FRA-JCOPE2, Miyazawa et al. 2009) uses the JCOPE2 ocean model, which is based on the Princeton Ocean Model with a generalized coordinate of sigma (Mellor et al. 2002) and provides daily mean ocean data covering the western North Pacific (10.5–62°N, 108–180°E) with a horizontal resolution of 1°/12°. The model assimilates the remote-sensing data of altimetry and surface temperature and in situ data of temperature and salinity profiles including the data from the FRA using the 3D-VAR method. Surface momentum and heat fluxes are calculated using the bulk formulae (Kagimoto et al. 2008) with atmospheric variables obtained from the National Centers for Environmental Prediction/National Center for Atmospheric Research (NCEP/NCAR) reanalysis (Kalnay et al. 1996). SSS is relaxed to monthly climatological data (Conkright et al. 2002). The FRA-JCOPE2 data set is provided by the Japan Agency for Marine-Earth Science and Technology (http://www.jamstec.go.jp/jcope/).

References

Abe H, Hanawa K, Ebuchi N (2013) Interannual variations in the Hawaiian Lee Countercurrent. J Oceanogr 69(2):191–202

Ambe D, Imawaki S, Uchida H, Ichikawa K (2004) Estimating the Kuroshio axis south of Japan using combination of satellite altimetry and drifting buoys. J Oceanogr 60:375–382

Andres M, Park J-H, Wimbush M, Zhu X-H, Chang K-I, Ichikawa H (2008) Study of the Kuroshio/Ryukyu Current system based on satellite-altimeter and in situ data measurements. J Oceanogr 64:937–950. doi:10.1007/s10872-008-0077-2

Antonov JI, Locarnini RA, Boyer TP, Mishonov AV, Garcia HE (2006) World Ocean Atlas 2005. In: Levitus S (ed) NOAA Atlas NESDIS 62. Salinity, vol 2. U.S. Government Printing Office, Washington, DC

Antonov JI, Seidov D, Boyer TP, Locarnini RA, Mishonov AV, Garcia HE, Baranova OK, Zweng MM, Johnson DR (2010) World Ocean Atlas 2009. In: Levitus S (ed) NOAA Atlas NESDIS 69. Salinity, vol 2. U.S. Government Printing Office, Washington, DC

Aoki Y, Suga T, Hanawa K (2002) Subsurface subtropical fronts of the North Pacific as inherent boundaries in the ventilated thermocline. J Phys Oceanogr 32:2299–2311

Beal L, de Ruijter WPM, Biastoch A, Zahn R, SCOR/WCRP/IAPSO Working Group 136 (2011) On the role of the Agulhas system in ocean circulation and climate. Nature 472:429–436

Belkin I, Krishfield R, Honjo S (2002) Decadal variability of the North Pacific polar front: subsurface warming versus surface cooling. Geophys Res Lett 29:1351. doi:10.1029/2001GL013806

Bernstein RL, White WB (1981) Stationary and traveling mesoscale perturbations in Kuroshio Extension current. J Phys Oceanogr 11:692–704

Bingham FM (1992) Formation and spreading of subtropical mode water in the North Pacific. J Geophys Res 97(C7):11177–11189. doi:10.1029/92JC01001

Book JW, Wimbush M, Imawaki S, Ichikawa H, Uchida H, Kinoshita H (2002) Kuroshio temporal and spatial variations south of Japan determined from inverted echo sounder measurements. J Geophys Res 107(C9):3121. doi:10.1029/2001JC000795

Bryden HL, Beal LM, Duncan LM (2005) Structure and transport of the Agulhas Current and its temporal variability. J Oceanogr 61:479–492

Chang Y-L, Oey L-Y (2014) Instability of the North Pacific Subtropical Countercurrent. J Phys Oceanogr 44. doi:10.1175/JPO-D-13-0162.1

Chang P-H, Guo X, Takeoka H (2009) A numerical study on the seasonal circulation in the Seto Inland Sea, Japan. J Oceanogr 65:721–736

Chelton DB, Schlax MG, Freilich MH, Milliff RF (2004) Satellite measurements reveal persistent small-scale features in ocean winds. Science 303(5660):978–983

Chen CTA (2009) Chemical and physical fronts in the Bohai, Yellow and East China Seas. J Mar Syst 78:394–410

Chu PC, Lan J, Fan C (2001) Japan Sea thermohaline structure and circulation. Part I: climatology. J Phys Oceanogr 31:244–271. doi:10.1175/1520-0485(2001)031<0244:JSTSAC>2.0.CO;2

Conkright ME, Antonov JI, Baranova O, Boyer TP, Garcia HE, Gelfeld R, Johnson D, Locarnini RA, Murphy PP, O'Brien TD, Smolyar I, Stephens C (2002) World Ocean Database 2001. In: Levitus S (ed) NOAA Atlas NESDIS 42. Introduction, vol 1. U.S. Government Printing Office, Washington, DC

Cromwell T, Reid JL (1956) A study of oceanic fronts. Tellus 8:94–101. doi:10.1111/j.2153-3490.1956.tb01198.x

Cunningham SA et al (2003) Transport and variability of the Antarctic Circumpolar Current in Drake Passage. J Geophys Res 108:8084. doi:10.1029/2001JC001147

Dinniman MS, Rienecker MM (1999) Frontogenesis in the North Pacific oceanic frontal zones: a numerical simulation. J Phys Oceanogr 29:537–559

Favorite F, Dodimead AJ, Nasu K (1976) Oceanography of the subarctic Pacific region, 1960-71. International North Pacific Fisheries Commission, Bulletin Number 33, 187 pp

Flament P, Kennan S, Lumpkin R et al (1998) The ocean. In: Juvik SP, Juvik JO (eds) Atlas of Hawaii. University of Hawaii Press, Honolulu, pp 82–86

Frankignoul C, Sennéchael N, Kwon YO, Alexander MA (2011) Influence of the meridional shifts of the Kuroshio and the Oyashio Extensions on the atmospheric circulation. J Clim 24:762–777. doi:10.1175/2010JCLI3731.1

Fujiwara I (1981) Oceanic features at the East China Sea: mean values of temperature, salinity and dissolved oxygen from 1951–1980. Mar Sci 13(4):264–270 (in Japanese)

Gentemann CL, Meissner T, Wentz FJ (2010) Accuracy of satellite sea surface temperatures at 7 and 11 GHz. IEEE Trans Geosci Remote Sens 48(3):1009–1018

Gordon AL (1985) Indian-Atlantic transfer of thermocline water at the Agulhas retroflection. Science 227:1030–1033

Gouretski V, Koltermann KP (2004) WOCE global hydrographic climatology. Berichte des BSH 35:1–52

Hayes SP, McPhaden MJ, Wallace JM (1989) The influence of sea-surface temperature on surface wind in the eastern equatorial Pacific: weekly to monthly variability. J Clim 2:1500–1506. doi:10.1175/1520-0442(1989)002<1500:TIOSST>2.0.CO;2

Hickox R, Belkin I, Cornillon P, Shan Z (2000) Climatology and seasonal variability of ocean fronts in the East China, Yellow and Bohai Seas from Satellite SST data. Geophys Res Lett 27:2945–2948

Hinata T (1996) Seasonal variation and long-term trends of the oceanographic conditions along a fixed hydrographic line crossing the Kuroshio in the East China Sea. Oceanogr Mag 45:9–32

Hofmann EE (1985) The large-scale horizontal structure of the Antarctic Circumpolar Current from FGGE drifters. J Geophys Res Oceans 90:7087–7097

Hogg NG (1992) On the transport of the Gulf Stream between Cape Hatteras and the Great Banks. Deep Sea Res 39:1231–1246

Hoskins B (2012) The potential for skill across the range of the seamless weather–climate prediction problem: a stimulus for our science. Q J R Meteorol Soc 139:573–584

Hotta D, Nakamura H (2011) On the significance of the sensible heat supply from the ocean in the maintenance of the mean baroclinicity along storm tracks. J Clim 24:3377–3401. doi:10.1175/2010JCLI3910.1

Howe PJ, Donohue KA, Watts DR (2009) Stream-coordinate structure and variability of the Kuroshio Extension. Deep Sea Res Part I Oceanogr Res Pap 56(7):1093–1116. doi:10.1016/j.dsr.2009.03.007

Hurlburt HE, Metzger EJ (1998) Bifurcation of the Kuroshio Extension at the Shatsky Rise. J Geophys Res 103:7549–7566

Hurlburt HE, Wallcraft AJ, Schmitz WJ, Hogan PJ, Metzger EJ (1996) Dynamics of the Kuroshio/Oyashio current system using an eddy resolving model of the North Pacific Ocean. J Geophys Res 101:951–976

Ichikawa H, Beardsley RC (1993) Temporal and spatial variability of volume transport of the Kuroshio in the East China Sea. Deep Sea Res I 40(3):583–605

Iizuka S (2010) Simulations of wintertime precipitation in the vicinity of Japan: sensitivity to fine-scale distributions of sea surface temperature. J Geophys Res 115:D10107. doi:10.1029/2009JD012576

Iizuka S, Shiota M, Kawamura R, Hatsushika H (2013) Influence of the monsoon variability and sea surface temperature front on the explosive cyclone activity in the vicinity of Japan during northern winter. SOLA 9:1–4. doi:10.2151/sola.2013-001

Imasato N, Qiu B (1987) An event in water exchange between continental shelf and the Kuroshio off southern Japan—Lagrangian tracking of a low-salinity water mass. J Phys Oceanogr 17:953–968

Imawaki S, Uchida H, Ichikawa H, Fukasawa M, Umatani S, The ASUKA Groups (2001) Satellite altimeter monitoring the Kuroshio Transport south of Japan. Geophys Res Lett 28:17–20

Imawaki S, Bower AS, Beal L, Qiu B (2013) Western Boundary Currents. In: Siedler G, Griffies S, Gould J, Church J (eds) Ocean circulation and climate: a 21st century perspective, Chapter 13, 2nd edn. Academic Press

Isobe A, Imawaki S (2002) Annual variation of the Kuroshio transport in a two-layer numerical model with a ridge. J Phys Oceanogr 32:994–1009

Isobe A, Isoda Y (1997) Circulation in the Japan Basin, the northern part of the Japan Sea. J Oceanogr 53:373–381

Isoda Y (1994) Interannual SST variations to the north and south of the polar front in the Japan Sea. La Mer 32:285–294

Isoda Y, Saitoh S, Mihara M (1991) SST structure of the polar front in the Japan Sea. In: Takano K (ed) Oceanography of Asian Marginal Seas. Elsevier Science Publisher, Amsterdam, pp 103–112

Isoguchi O, Kawamura H, Oka E (2006) Quasi-stationary jets transporting surface warm waters across the transition zone between the subtropical and the subarctic gyres in the North Pacific. J Geophys Res 111:C10003. doi:10.1029/2005JC003402

Itoh S, Yasuda I (2010) Characteristics of mesoscale eddies in the Kuroshio–Oyashio Extension region detected from the distribution of the sea surface height anomaly. J Phys Oceanogr 40:1018–1034

Jacobs GA, Hogan PJ, Whitmer KR (1999) Effects of eddy variability on the circulation of the Japan/East Sea. J Oceanogr 55(2):247–256

Johns WE, Shay TJ, Bane JM, Watts DR (1995) Gulf Stream structure, transport, and recirculation near 68°W. J Geophys Res 100:817–838

Joyce TM, Jenkins WJ (1993) Spatial variability of subducting water in the North Atlantic: a pilot study. J Geophys Res 98(C6):10111–10124. doi:10.1029/93JC00572

Joyce TM, Kwon YO, Yu L (2009) On the relationship between synoptic wintertime atmospheric variability and path shifts in the Gulf Stream and the Kuroshio Extension. J Clim 22:3177–3192

Kagimoto T, Yamagata T (1997) Seasonal transport variations of the Kuroshio: an OGCM simulation. J Phys Oceanogr 27:403–418

Kagimoto T, Miyazawa Y, Guo X, Kawajiri H (2008) High resolution Kuroshio forecast system—description and its applications. In: Ohfuchi W, Hamilton K (eds) High resolution numerical modeling of the atmosphere and ocean. Springer, New York, pp 209–234

Kalnay E et al (1996) The NCEP/NCAR 40-year reanalysis project. Bull Am Meteorol Soc 77:437–471

Kasamo K, Isobe A, Minobe S, Manda A, Nakamura H, Ogata K, Nishikawa H, Tachibana Y, Kako S (2014) Transient and local weakening of surface winds observed above the Kuroshio front in the winter East China Sea. J Geophys Res Atmos 119:1277–1291. doi:10.1002/2013JD020610

Kawabe M (1987) Spectral properties of sea level and time scale of Kuroshio path variations. J Oceanogr Soc Jpn 43:111–123

Kawabe M (1988) Variability of Kuroshio velocity assessed from the sea-level difference between Naze and Nishinoomote. J Oceanogr Soc Jpn 44:293–304

Kawabe M (1995) Variations of current path, velocity, and volume transport of the Kuroshio in relation with the large meander. J Phys Oceanogr 25:3103–3117

Kawai H (1969) Statistical estimation of isotherms indicative of the Kuroshio axis. Deep Sea Res 16(Suppl):109–115

Kawai H (1972) Hydrography of the Kuroshio Extension. In: Stommel H, Yoshida K (eds) Kuroshio, its physical aspects. University of Tokyo Press, Tokyo, pp 235–352

Kawai Y, Miyama T, Iizuka S, Manda A, Yoshioka M K, Katagiri S, Tachibana Y, Nakamura H (2014) Marine atmospheric boundary layer and low-level cloud responses to the Kuroshio Extension front in the early summer of 2012: three-vessel simultaneous observations and numerical simulations. J Oceanogr 70. doi:10.1007/s10872-014-0266-0

Kazmin AS, Rienecker MM (1996) Variability and frontogenesis in the large-scale oceanic frontal zones. J Geophys Res 101:907–921

Kelly KA, Small RJ, Samelson RM, Qiu B, Joyce TM, Kwon YO, Cronin MF (2010) Western boundary currents and frontal air–sea interaction: Gulf Stream and Kuroshio Extension. J Clim 23:5644–5667. doi:10.1175/2010JCLI3346.1

Kimura K (1949) Maps of fishing grounds of skipjack. Kuroshio Shobou, Tokyo (in Japanese)

Kitahara T (1921) Collision of ocean currents. In: Kitahara T (ed) Ocean study: night fable of fishery village. Dai-Nihon-Suisan-Kai, Tokyo, pp 303–310 (in Japanese)

Kobashi F, Kawamura H (2002) Seasonal variation and instability nature of the North Pacific Subtropical Countercurrent and the Hawaiian Lee Countercurrent. J Geophys Res 107:3185. doi:10.1029/2001JC001225

Kobashi F, Kubokawa A (2012) Review on North Pacific Subtropical Countercurrents and subtropical fronts: Role of mode waters in ocean circulation and climate. J Oceanogr 68:21–43. doi:10.1007/s10872-011-0083-7

Kobashi F, Mitsudera H, Xie S-P (2006) Three subtropical fronts in the North Pacific: observational evidence for mode water-induced subsurface frontogenesis. J Geophys Res 111:C09033. doi:10.1029/2006JC003479

Kobashi F, Xie S-P, Iwasaka N, Sakamoto TT (2008) Deep atmospheric response to the North Pacific oceanic subtropical front in spring. J Clim 21:5960–5975

Kubokawa A (1999) Ventilated thermocline strongly affected by a deep mixed layer: a theory for subtropical countercurrent. J Phys Oceanogr 29:1314–1333

Kubota M, Iwasaka N, Kizu S, Konda M, Kutsuwada K (2002) Japanese ocean flux datasets with use of remote sensing observations (J-OFURO). J Oceanogr 58:213–225

Kurihara Y, Sakurai T, Kuragano T (2000) Global daily sea surface temperature analysis using data from satellite microwave radiometer, satellite infrared radiometer and in situ observations. Weather Bull 73:s1–s18 (in Japanese)

Kuwano-Yoshida A, Enomoto T, Ohfuchi W (2010) An improved PDF cloud scheme for climate simulations. Q J R Meteorol Soc 136(651):1583–1597

Kwon Y, Alexander MA, Bond NA, Frankignoul C, Nakamura H, Qiu B, Thompson L (2010) Role of the Gulf Stream and Kuroshio–Oyashio systems in large-scale atmosphere–ocean interaction: a review. J Clim 23:3249–3281. doi:10.1175/2010JCLI3343.1

Lee CM, Thomas LN, Yoshikawa Y (2006) Intermediate water formation. Oceanography 19(3):110

Lindzen RS, Nigam S (1987) On the role of sea surface temperature gradients in forcing low-level winds and convergence in the tropics. J Atmos Sci 44:2418–2436. doi:10.1175/1520-0469(1987)044<2418:OTROSS>2.0.CO;2

Liu WT, Xie X, Niiler PP (2007) Ocean–atmosphere interaction over Agulhas extension meanders. J Clim 20:5784–5797. doi:10.1175/2007JCLI1732.1

Lumpkin R, Flament PJ (2013) Extent and energetics of the Hawaiian Lee Countercurrent. Oceanography 26(1):58–65. doi:10.5670/oceanog.2013.05

Lutjeharms JRE, Ansorge IJ (2001) The Agulhas Return Current. J Mar Syst 30:115–138

Masumoto Y, Sasaki H, Kagimoto T, Komori N, Ishida A, Sasai Y, Miyama T, Motoi T, Mitsudera H, Takahashi K, Sakuma H, Yamagata T (2004) A fifty-year eddy-resolving simulation of the world ocean—preliminary outcomes of OFES (OGCM for the Earth Simulator). J Earth Simul 1:35–56

Masunaga R, Nakamura H, Miyasaka T, Nishii K, Tanimoto Y (2014) Separation of climatological imprints of the Kuroshio Extension and Oyashio fronts on the wintertime atmospheric boundary layer: their sensitivity to SST resolution prescribed for atmospheric reanalysis. J Clim 28:1764–1787. doi:10.1175/JCLI-D-14-00314.1

Mellor GL, Hakkinen S, Ezer T, Patchen R (2002) A generalization of a sigma coordinate ocean model and an intercomparison of model vertical grids. In: Pinardi N, Woods JD (eds) Ocean forecasting: conceptual basis and applications. Springer, New York, pp 55–72

Minobe S, Sako A, Nakamura M (2004) Interannual to interdecadal variability in the Japan Sea based on a new gridded upper water temperature dataset. J Phys Oceanogr 34:2382–2397. doi:10.1175/JPO2627.1

Minobe S, Kuwano-Yoshida A, Komori N, Xie SP, Small RJ (2008) Influence of the Gulf Stream on the troposphere. Nature 452:206–209

Minobe S, Miyashita M, Kuwano-Yoshida A, Tokinaga H, Xie SP (2010) Atmospheric response to the Gulf Stream: seasonal variations. J Clim 23:3699–3719. doi:10.1175/2010JCLI3359.1

Miyama T, Nonaka M, Nakamura H, Kuwano-Yoshida A (2012) A striking early-summer event of a convective rainband persistent along the warm Kuroshio in the East China Sea. Tellus-A 64:18962. doi:10.3402/tellusa.v64i0.18962

Miyasaka T, Nakamura H (2010) Structure and mechanism of the Southern Hemisphere summertime subtropical anticyclones. J Clim 23:2115–2130

Miyazawa Y, Guo X, Yamagata T (2004) Roles of mesoscale eddies in the Kuroshio paths. J Phys Oceanogr 34:2203–2222. doi:10.1175/1520-0485(2004)034<2203:ROMEIT>2.0.CO;2

Miyazawa Y, Zhang R, Guo X, Tamura H, Ambe D, Lee JS, Okuno A, Yoshinari H, Setou T, Komatsu K (2009) Water mass variability in the western North Pacific detected in a 15-year eddy resolving ocean reanalysis. J Oceanogr 65(6):737–756

Mizuno K, White WB (1983) Annual and interannual variability in the Kuroshio Current system. J Phys Oceanogr 13:1848–1869

Murakami M (1993) On the 100 meter depth temperature indicative of the Kuroshio Extension axis in Tohoku area. Umi no Kenkyu 2:343–349 (in Japanese with English abstract)

Nakamura H (2012) A latest development in extratropical climate research: warm western boundary currents and associated oceanic fronts as “hotspots in the climate system” (in Japanese). Japan Geosci Lett 8(4):1–4 (see also http://www.atmos.rcast.u-tokyo.ac.jp/hotspot/index_eng.html)

Nakamura H, Kazmin A (2003) Decadal changes in the North Pacific frontal zones as revealed in ship and satellite observations. J Geophys Res 108:C33078

Nakamura H, Shimpo A (2004) Seasonal variations in the Southern Hemisphere storm tracks and jet streams as revealed in a reanalysis dataset. J Clim 17:1828–1844. doi:10.1175/1520-0442(2004)017<1828:SVITSH>2.0.CO;2

Nakamura H, Yamagata T (1999) Recent decadal variability in the northwestern Pacific and associated atmospheric anomaly. In: Navvara A (ed) Beyond El Nino: decadal and interdecadal climate variability. Springer, New York, pp 49–72

Nakamura H, Lin G, Yamagata T (1997) Decadal climate variability in the North Pacific during the recent decades. Bull Am Meteorol Soc 78:2215–2225. doi:10.1175/1520-0477(1997)078<2215:DCVITN>2.0.CO;2

Nakamura H, Sampe T, Tanimoto Y, Shimpo A (2004) Observed associations among storm tracks, jet streams and midlatitude oceanic fronts. In: Wang C, Xie S-P, Carton JA (eds) Earth's climate: the ocean–atmosphere interaction. Geophys Monogr 147, AGU, pp 329–345

Nakamura H, Sampe T, Goto A, Ohfuchi W, Xie SP (2008) On the importance of midlatitude oceanic frontal zones for the mean state and dominant variability in the tropospheric circulation. Geophys Res Lett 35:L15709. doi:10.1029/2008GL034010

Nakamura H, Miyasaka T, Kosaka Y, Takaya K, Honda M (2010) Northern Hemisphere extratropical tropospheric planetary waves and their low-frequency variability: their vertical structure and interaction with transient eddies and surface thermal contrasts. In: Sun D, Bryan F (eds) Climate dynamics: why does climate vary? chap 6. Geophys Monogr 189, AGU, pp 149–179

Nakamura H, Nishina A, Minobe S (2012) Response of storm tracks to bimodal Kuroshio path states south of Japan. J Clim 25:7772–7779

Nakano T, Takatsuki Y, Kaneko I (1994) The Kuroshio structure and transport estimated by the inverse method. J Phys Oceanogr 24:609–618

Nakano H, Tsujino H, Furue R (2008) The Kuroshio Current System as a jet and twin "relative" recirculation gyres embedded in the Sverdrup circulation. Dyn Atmos Ocean 45:135–164

Niiler PP, Maximenko NA, Panteleev GG, Yamagata T, Olson DB (2003a) Near-surface dynamical structure of the Kuroshio Extension. J Geophys Res 108(C6):3193. doi:10.1029/2002JC001461

Niiler PP, Maximenko NA, McWilliams JC (2003b) Dynamically balanced absolute sea level of the global ocean derived from near-surface velocity observations. Geophys Res Lett 30(22):2164. doi:10.1029/2003GL018628

Nonaka M, Nakamura H, Tanimoto Y, Kagimoto T, Sasaki H (2006) Decadal variability in the Kuroshio–Oyashio Extension simulated in an eddy-resolving OGCM. J Clim 19(10):1970–1989. doi:10.1175/JCLI3793.1

Nonaka M, Nakamura H, Taguchi B, Komori N, Kuwano-Yoshida A, Takaya K (2009) Air–sea heat exchanges characteristic of a prominent midlatitude oceanic front in the South Indian Ocean as simulated in a high-resolution coupled GCM. J Clim 22:6515–6535

O'Reilly CH, Czaja A (2014) The response of the Pacific storm track and atmospheric circulation to Kuroshio Extension variability. Q J R Meteorol Soc. doi:10.1002/qj.2334

Ogawa F, Nakamura H, Nishii K, Miyasaka T, Kuwano-Yoshida A (2012) Dependence of the climatological axial latitudes of the tropospheric westerlies and storm tracks on the latitude of an extratropical oceanic front. Geophys Res Lett 39. doi:10.1029/2011GL049922

Ohtani K (1970) Relative transport in the Alaskan Stream in winter. J Oceanogr Soc Jpn 26:271–282

Oka E, Kawabe M (1998) Characteristics of variations of water properties and density structure around the Kuroshio in the East China Sea. J Oceanogr 54:605–617

Oka E, Qiu B (2012) Progress of North Pacific mode water research in the past decade. J Oceanogr 68:5–20. doi:10.1007/s10872-011-0032-5

Oka E, Koketsu S, Toyama K, Uehara K, Kobayashi T, Hosoda S, Suga T (2011) Formation and subduction of central mode water based on profiling float data, 2003-08. J Phys Oceanogr 41:113–129. doi:10.1175/2010JPO4419.1

Okajima S, Nakamura H, Nishii K, Miyasaka T, Kuwano-Yoshida A (2014) Assessing the importance of prominent warm SST anomalies over the midlatitude north pacific in forcing large-scale atmospheric anomalies during 2011 summer and autumn. J Clim 27:3889–3903. doi:10.1175/JCLI-D-13-00140.1

Orsi AH, Whitworth T, Nowlin WD (1995) On the meridional extent and fronts of the Antarctic Circumpolar Current. Deep Sea Res I 42:641–673

Park K-A, Chung JY, Kim K (2004) Sea surface temperature fronts in the East (Japan) Sea and temporal variations. Geophys Res Lett 31(L07304). doi:10.1029/2004GL019424

Patterson SL (1985) Surface circulation and kinetic energy distributions in the Southern Hemisphere Oceans from FGGE drifting buoys. J Phys Oceanogr 15:865–884

Pollard RT, Regier LA (1992) Vorticity and vertical circulation at an ocean front. J Phys Oceanogr 22:609–625. doi:10.1175/1520-0485(1992)022<0609:VAVCAA>2.0.CO;2

Qiu B (1999) Seasonal eddy field modulation of the North Pacific subtropical countercurrent: TOPEX/Poseidon observations and theory. J Phys Oceanogr 29:2471–2486

Qiu B, Chen S (2005) Variability of the Kuroshio Extension jet, recirculation gyre, and mesoscale eddies on decadal time series. J Phys Oceanogr 35:2090–2103

Qiu B, Chen S (2010a) Eddy-mean flow interaction in the decadally modulating Kuroshio Extension system. Deep Sea Res 57:1098–1110

Qiu B, Chen S (2010b) Interannual variability of the North Pacific Subtropical Countercurrent and its associated mesoscale eddy field. J Phys Oceanogr 40:213–225

Qiu B, Chen S (2013) Concurrent decadal mesoscale eddy modulations in the western North Pacific subtropical gyre. J Phys Oceanogr 43:344–358

Qiu C, Kawamura H (2012) Study on SST front disappearance in the subtropical North Pacific using microwave SSTs. J Oceanogr 68:417–426. doi:10.1007/s10872-012-0106-z

Qiu B, Toda T, Imasato N (1990) On Kuroshio front fluctuations in the East China Sea using satellite and in situ observational data. J Geophys Res 95:18191–18204

Qiu B, Kelly KA, Joyce TM (1991) Mean flow and variability in the Kuroshio Extension from Geosat altimetry data. J Geophys Res 96:18491–18507

Qiu B, Koh DA, Lumpkin C, Flament P (1997) Existence and formation mechanism of the North Hawaiian Ridge Current. J Phys Oceanogr 27:431–444. doi:10.1175/1520-0485(1997)027<0431:EAFMOT>2.0.CO;2

Qiu B, Chen S, Hacker P, Hogg N, Jayne S, Sasaki H (2008) The Kuroshio Extension northern recirculation gyre: profiling float measurements and forcing mechanism. J Phys Oceanogr 38:1764–1779

Reynolds RW, Rayner NA, Smith TM, Stokes DC, Wang W (2002) An improved in situ and satellite SST analysis for climate. J Clim 15:1609–1625

Reynolds RW, Smith TM, Liu C, Chelton DB, Casey KS, Schlax MG (2007) Daily high-resolution blended analyses for sea surface temperature. J Clim 20:5473–5496

Rintoul SR, Naveira Garabato AC (2013) Dynamics of the Southern Ocean circulation. In: Siedler G, Griffies SM, Gould J, Church JA (eds) Ocean circulation and climate. International geophysics series, vol 103. Academic Press Oxford, UK, pp 471–492

Rintoul SR, Sokolov S (2001) Baroclinic transport variability of the Antarctic Circumpolar Current south of Australia (WOCE repeat section SR3). J Geophys Res 106:2815–2832

Rio M-H, Guinehut S, Larnicol G (2011) New CNES-CLS09 global mean dynamic topography computed from the combination of GRACE data, altimetry, and in situ measurements. J Geophys Res 116:C07018. doi:10.1029/2010JC006505

Roden GI (1980) On the variability of surface temperature fronts in the western Pacific, as detected by satellite. J Geophys Res 85:2704–2710

Roden GI, Taft BA, Ebbesmeyer CC (1982) Oceanographic aspects of the Emperor Seamounts region. J Geophys Res 87:9537–9552

Sallee JB, Speer K, Morrow R (2008) Response of the Antarctic Circumpolar Current to atmospheric variability. J Clim 21:3020–3039

Sampe T, Nakamura H, Goto A, Ohfuchi W (2010) Significance of a midlatitude SST frontal zone in the formation of a storm track and an eddy-driven westerly jet. J Clim 23:1793–1814. doi:10.1175/2009JCLI3163.1

Sasaki YN, Schneider N (2011) Interannual to decadal Gulf Stream variability in an eddy-resolving ocean model. Ocean Model 39:209–219

Sasaki H, Nonaka M, Masumoto Y, Sasai Y, Uehara H, Sakuma H (2008) An eddy-resolving hindcast simulation of the quasi global ocean from 1950 to 2003 on the Earth Simulator. In: Hamilton K, Ohfuchi W (eds) High resolution numerical modelling of the atmosphere and ocean, chap 10. Springer, New York, pp 157–185

Sasaki H, Xie S-P, Taguchi B, Nonaka M, Masumoto Y (2010) Seasonal variations of the Hawaiian Lee Countercurrent induced by the meridional migration of the Trade Winds. Ocean Dyn 60(3):705–715

Sasaki YN, Minobe S, Asai T, Inatsu M (2012a) Influence of the Kuroshio in the East China Sea on the Early Summer (Baiu) Rain. J Clim 25:6627–6645. doi:10.1175/JCLI-D-11-00727.1

Sasaki H, Xie S-P, Taguchi B, Nonaka M, Hosoda S, Masumoto Y (2012b) Interannual variations of the Hawaiian Lee Countercurrent induced by low potential vorticity water ventilation in the subsurface. J Oceanogr 68:93–111

Sasaki H, Taguchi B, Komori N, Masumoto Y (2013) Influence of local dynamical air–sea feedback process on the Hawaiian Lee Countercurrent. J Clim 26(18):7267–7279

Schneider N, Miller AJ, Pierce DW (2002) Anatomy of North Pacific decadal variability. J Clim 15:586–605

Seo Y, Sugimoto S, Hanawa K (2014a) Long-term variations of the Kuroshio Extension path in winter: meridional movement and path state change. J Clim 27:5929–5940. doi:10.1175/JCLI-D-13-00641.1

Seo H, Kwon Y-O, Park J-J (2014b) On the effect of the East/Japan Sea SST variability on the North Pacific atmospheric circulation in a regional climate model. J Geophys Res Atmos 119:418–444. doi:10.1002/2013JD020523

Shi R, Guo X, Takeoka H (2011) Influences of tidal fronts on coastal winds over an Inland Sea. Bound Layer Meteorol 138:299–319

Shimada T, Kawamura H (2006) Satellite observations of sea surface temperature and sea surface wind coupling in the Japan Sea. J Geophys Res 111:C08010. doi:10.1029/2005JC003345

Shimada T, Kawamura H (2008) Satellite evidence of wintertime atmospheric boundary layer responses to multiple SST fronts in the Japan Sea. Geophys Res Lett 35:L23602. doi:10.1029/2008GL035810

Shimada T, Minobe S (2011) Global analysis of the pressure adjustment mechanism over sea surface temperature fronts using AIRS/Aqua data. Geophys Res Lett 38:L06704. doi:10.1029/2010GL046625

Shimada T, Sakaida F, Kawamura H (2005) Application of an edge detection method to satellite images for distinguishing sea surface temperature fronts near the Japanese coast. Remote Sens Environ 98:21–34

Simpson JH, Hunter JR (1974) Fronts in the Irish Sea. Nature 250:404–406

Small RJ, DeSzoeke SP, Xie SP, O'Neill L, Seo H, Song Q, Cornillon P, Spall M, Minobe S (2008) Air–sea interaction over ocean fronts and eddies. Dyn Atmos Oceans 45(3):274–319. doi:10.1016/j.dynatmoce.2008.01.001

Smirnov D, Newman M, Alexander MA, Kwon Y-O, Frankignoul C (2015) Investigating the local atmospheric response to a realistic shift in the Oyashio sea surface temperature front. J Clim 28:1126–1147

Sokolov S, Rintoul SR (2007) Multiple jets of the Antarctic Circumpolar Current South of Australia. J Phys Oceanogr 37:1394–1412. doi:10.1175/JPO3111.1

Spall MA (1995) Frontogenesis, subduction, and cross-front exchange at upper ocean fronts. J Geophys Res 100(C2):2543–2557. doi:10.1029/94JC02860

Suga T, Takei Y, Hanawa K (1997) Thermostat distribution in the North Pacific subtropical gyre: the central mode water and the subtropical mode water. J Phys Oceanogr 27:140–152

Suga T, Motoki K, Aoki Y, MacDonald AM (2004) The North Pacific climatology of winter mixed layer and mode waters. J Phys Oceanogr 34:3–22

Suga T, Aoki Y, Saito H, Hanawa K (2008) Ventilation of the North Pacific subtropical pycnocline and mode water formation. Prog Oceanogr 77:285–297. doi:10.1016/j.pocean.2006.12.005

Sugimoto S, Hanawa K (2011) Roles of SST anomalies on the wintertime turbulent heat fluxes in the Kuroshio–Oyashio confluence region: influences of warm eddies detached from the Kuroshio Extension. J Clim 24:6551–6561

Sugimoto S, Hanawa K (2012) Relationship between the path of the Kuroshio in the south of Japan and the path of the Kuroshio Extension in the east. J Oceanogr 68:219–225

Sun Y-J, Isobe A (2006) Numerical study of tidal front with varying sharpness in spring and neap tidal cycle. J Oceanogr 62:801–810

Taguchi B, Nakamura H, Nonaka M, Xie SP (2009) Influences of the Kuroshio/Oyashio Extensions on air–sea heat exchanges and storm-track activity as revealed in regional as revealed in regional atmospheric model simulations for the 2003/04 cold season. J Clim 22:6536–6560

Taguchi B, Nakamura H, Nonaka M, Komori N, Kuwano-Yoshida A, Takaya K, Goto A (2012) Seasonal evolutions of atmospheric response to decadal SST anomalies in the North Pacific Subarctic Frontal Zone: observations and a coupled model simulation. J Clim 25:111–139. doi:10.1175/JCLI-D-11-00046.1

Takeoka H (2002) Progress in Seto Inland Sea research. J Oceanogr 58:93–107

Talley LD, Nagata Y, Fujimura M, Iwao T, Kono T, Inagake D, Hirai M, Okuda K (1995) North Pacific intermediate water in the Kuroshio/Oyashio mixed water region. J Phys Oceanogr 25:475–501

Talley LD, Min D-H, Lobonov VB, Luchin VA, Ponomarev VI, Salyuk AN, Shcherbina AY, Tishcenko PY, Zhabin I (2006) Japan/East Sea water masses and their relation to the sea's circulation. Oceanography 19:32–49

Talley LD, Pickard GL, Emery WJ, Swift JH (2011) Descriptive physical oceanography: an introduction. Academic Press, New York

Tanimoto Y, Nakamura H, Kagimoto T, Yamane S (2003) An active role of extratropical sea surface temperature anomalies in determining anomalous turbulent heat flux. J Geophys Res 108:3304. doi:10.1029/2002JC001750

Tanimoto Y, Xie SP, Kai K, Okajima H, Tokinaga H, Murayama T, Nonaka M, Nakamura H (2009) Observations of marine atmospheric boundary layer transitions across the summer Kuroshio Extension. J Clim 22:1360–1374

Tanimoto Y, Kanenari T, Tokinaga H, Xie SP (2011) Sea level pressure minimum along the Kuroshio and its extension. J Clim 24:4419–4434. doi:10.1175/2011JCLI4062.1

Tatebe H, Yasuda I (2001) Seasonal axis migration of the upstream Kuroshio Extension associated with standing oscillations. J Geophys Res 106(C8):16685–16692

Thomas LN, Lee CM (2005) Intensification of ocean fronts by downfront winds. J Phys Oceanogr 35:1086–1102

Tokinaga H, Tanimoto Y, Xie SP, Sampe T, Tomita H, Ichikawa H (2009) Ocean frontal effects on the vertical development of clouds over the Western North Pacific: in situ and satellite observations. J Clim 22:4241–4260. doi:10.1175/2009JCLI2763.1

Tomczak M, Godfrey JS (2003) Regional oceanography: an introduction, 2nd edn. http://www.es.flinders.edu.au/~mattom/regoc/pdfversion.html

Tomita H, Kubota M, Cronin MF, Iwasaki S, Konda M, Ichikawa H (2010) An assessment of surface heat fluxes from J-OFURO2 at the KEO and JKEO sites. J Geophys Res 115:C03018. doi:10.1029/2009JC005545

Tomita H, Kouketsu S, Oka E, Kubota M (2011) Locally enhanced wintertime air–sea interaction and deep oceanic mixed layer formation associated with the subarctic front in the North Pacific. Geophys Res Lett 38:L24607. doi:10.1029/2011GL049902

Tozuka T, Cronin MF (2014) Role of mixed layer depth in relaxation of the Agulhas Return Current surface front. Geophys Res Lett 41:2447–2453. doi:10.1002/2014GL059624

Tsujino H, Nishikawa S, Sakamoto K, Usui N, Nakano H, Yamanaka G (2013) Effects of large-scale wind on the Kuroshio path south of Japan in a 60-year historical OGCM simulation. Clim Dyn 41:2287–2318. doi:10.1007/s00382-012-1641-4

Uda M (1938) Researches on 'Siome' or current rip in the seas and oceans. Geophys Mag 11(4):307–372

Uda M, Hasunuma K (1969) The eastward subtropical countercurrent in the western North Pacific Ocean. J Oceanogr Soc Jpn 25:201–210

Ueno H, Yasuda I (2000) Distribution and formation of the mesothermal structure (temperature inversions) in the North Pacific subarctic region. J Geophys Res 105:16885–16897

Usui N, Tsujino H, Nakano H, Matsumoto S (2013) Long-term variability of the Kuroshio path south of Japan. J Oceanogr 69(6):647–670

Wagawa T, Ito S, Shimizu Y, Kakehi S, Ambe D (2014) Currents associated with the quasi-stationary jet separated from the Kuroshio Extension. J Phys Oceanogr 44:1636–1653. doi:10.1175/JPO-D-12-0192.1

Wallace JM, Mitchell TP, Deser C (1989) The influence of sea-surface temperature on surface wind in the eastern equatorial Pacific: seasonal and interannual variability. J Clim 2:1492–1499. doi:10.1175/1520-0442(1989)002<1492:TIOSST>2.0.CO;2

Waterman S, Hogg N, Jayne S (2011) Eddy-mean flow interaction in the Kuroshio Extension region. J Phys Oceanogr 41:1182–1208

Xie SP (2004) Satellite observations of cool ocean–atmosphere interaction. Bull Am Meteorol Soc 85:195–208. doi:10.1175/BAMS-85-2-195

Xie S-P, Liu WT, Liu Q, Nonaka M (2001) Far-reaching effects of the Hawaiian Islands on the Pacific ocean–atmosphere system. Science 292:2057–2060

Xie SP, Hafner J, Tanimoto Y, Liu WT, Tokinaga H, Xu H (2002) Bathymetric effect on the winter sea surface temperature and climate of the Yellow and East China Seas. Geophys Res Lett 29(24):2228. doi:10.1029/2002GL015884

Xie S-P, Xu L-X, Liu Q, Kobashi F (2011) Dynamical role of mode-water ventilation in decadal variability in the central subtropical gyre of the North Pacific. J Clim 24:1212–1225

Yamamoto M, Hirose N (2011) Possible modification of atmospheric circulation over the northwestern Pacific induced by a small semi-enclosed ocean. Geophys Res Lett 38:L03804. doi:10.1029/2010GL046214

Yanagi T (1987) Classification of "siome", streaks and fronts. J Oceanogr Soc Jpn 43(3):149–158

Yanagi T, Koike T (1987) Seasonal variation in thermohaline and tidal fronts, Seto Inland Sea, Japan. Cont Shelf Res 7:149–160

Yasuda I (2003) Hydrographic structure and variability in the Kuroshio–Oyashio transition area. J Oceanogr 59:389–402

Yasuda I, Okuda K, Shimizu Y (1996) Distribution and modification of North Pacific intermediate water in the Kuroshio–Oyashio interfrontal zone. J Phys Oceanogr 26:448–465

Yoshida S, Qiu B, Hacker P (2011) Low-frequency eddy modulations in the Hawaiian Lee Countercurrent: observations and connection to the Pacific Decadal Oscillation. J Geophys Res 116:C12009. doi:10.1029/2011JC007286

Yoshikawa Y, Akitomo K, Awaji T (2001) Formation process of intermediate water in baroclinic current under cooling. J Geophys Res 106:1033–1051

Yu L, Weller RA (2007) Objectively analyzed air–sea heat fluxes for the global ice-free oceans (1981–2005). Bull Am Meteorol Soc 88:527–539. doi:10.1175/BAMS-88-4-527

Yu Z, Maximenko N, Xie S-P, Nonaka M (2003) On the termination of the Hawaiian Lee Countercurrent. Geophys Res Lett 30(5):1215. doi:10.1029/2002GL016710

Yuan X, Talley LD (1996) The subarctic frontal zone in the North Pacific: characteristics of frontal structure from climatological data and synoptic surveys. J Geophys Res 101:16491–16508

Zhang R-C, Hanawa K (1993) Features of the water-mass front in the northwestern North Pacific. J Geophys Res 98:967–975

Zweng MM, Reagan JR, Antonov JI, Locarnini RA, Mishonov AV, Boyer TP, Garcia HE, Baranova OK, Johnson DR, Seidov D, Biddle MM (2013) World Ocean Atlas 2013. In: Levitus S (ed), Mishonov A (Technical ed) Salinity, vol 2. NOAA Atlas NESDIS 74